

# Vanishing Beta Function curves from the Functional Renormalisation Group

P. Mati

*MTA-DE Particle Physics Research Group, P.O.Box 51, H-4001 Debrecen, Hungary  
Budapest University of Technology and Economics, H-1111 Budapest, Hungary and  
Eötvös University, H-1117 Budapest, Hungary*

In this paper we will discuss the derivation of the so called Vanishing Beta Function curves which can be used to explore the fixed point structure of the theory under consideration. This can be applied to the  $O(N)$  symmetric theories essentially for arbitrary dimensions ( $D$ ) and field component ( $N$ ). We will show the restoration of the Mermin-Wagner theorem for theories defined in  $D \leq 2$  and the presence of the Wilson Fisher fixed point in  $2 < D < 4$ . Triviality is found in  $D > 4$ . Interestingly, one needs to make an excursion to the complex plane to see the triviality of the four dimensional  $O(N)$  theories. The large  $N$  analysis shows a new fixed point candidate in  $4 < D < 6$  dimensions which turns out to define an unbounded fixed point potential supporting the recent results by R. Percacci and G. P. Vacca in: "Are there scaling solutions in the  $O(N)$ -models for large  $N$  in  $D > 4$ ?" ([13]).

PACS numbers: 11.10.Gh, 11.10.Hi, 05.10.Cc, 11.10.Kk

## I. INTRODUCTION

There have been many investigations on the phase structure of the scalar  $O(N)$  models [1–5] using functional renormalisation group (FRG) techniques [6, 8, 9] in various dimensions. Critical exponents were computed with high precision, fixed points were found, many physical aspects seem to be well understood. Hence we can safely state: the FRG method is a reliable tool for non-perturbative calculations which can be used to consider the phase structure of a model and consequently to study e.g. the appearance of spontaneous symmetry breaking (SSB). For instance, according to the Mermin-Wagner theorem [18–20] a continuous symmetry cannot be broken spontaneously below a lower critical dimension, which is  $D = 2$  for the  $O(N)$  symmetric scalar theory for  $N > 2$ , and this has been recently shown in the framework of FRG [22]. A numerical evidence for the MW theorem is presented in [23]. In summary we can say that the  $O(N)$  scalar model represents an excellent playground for testing new techniques. The goal of this paper is to introduce the so called Vanishing Beta Function (VBF) method in the framework of the  $O(N)$  symmetric scalar field theory, where the Wetterich FRG equation [6] is used in the Local Potential Approximation (LPA) assuming that the potential is analytic around the vanishing field. There is an extensive study about the radius of convergence of the Taylor-expanded effective potential in the large  $N$  limit of the  $O(N)$  model in [17]. Expanding around vanishing field enables us to provide a one-parameter representation of the fixed point solution which actually defines the VBF curves through the couplings. This single parameter is the quadratic coupling of the theory ( $m^2$ ) and the roots of the VBF curve will define the position of the fixed points at a given truncation level. In this approach we will lay down general requirements that a root must satisfy in order to define a stable fixed point potential. Using this polynomial expression for the couplings will reveal an interesting root structure, which depends highly on dimensionality but there is a dependence on  $N$ , too, which is rather quantitative. As a consequence of the approximations used in the VBF technique could lead us to potentially artificial fixed points even in the higher order of truncation. However, it can be shown that these "spurious" fixed point solutions are excluded by taking the infinite limit in the order of the expansion, although strict mathematically they must be considered as a valid fixed point at finite truncation. We will show, from a different aspect that has been used in [22] and [23], that the Mermin-Wagner theorem is not violated, although at finite truncation order one would draw the opposite conclusion. Equally interesting finding is the direct observation of triviality above four Euclidean dimensions, however for  $D = 4$  triviality can be found only if we track down the root structure on the complex plane, too. In theories  $4 < D < 6$  a new fixed point candidate is found in the large  $N$  limit, a detailed analysis is shown for the  $D = 5$  case. However, it turns out that this fixed point defines an unbounded potential from below in agreement with the findings in [13]. In the last two sections we will analyse the  $N$  dependence and some fractal dimensional results are presented, too.

### A. The Functional Renormalisation Group

The effective average action of an  $O(N)$  symmetric scalar field theory in  $D$  Euclidean dimensions using the LPA approximation will have the following form

$$\Gamma_k = \int d^D x \left[ \frac{1}{2} (\partial \bar{\phi})^2 + U_k(\bar{\phi}^2) \right]. \quad (1)$$

$U_k$  is the dimensionful potential that depends only on the  $O(N)$  invariant terms of the theory, namely on  $\bar{\phi}^2$ , where  $\bar{\phi}$  is the vacuum expectation value (VEV) of the field. The subscript  $k$  stands for the RG scale (i.e. the Wilsonian cutoff), on which the effective theory is being defined. The dependence of Eq.(1) on the RG scale parameter  $k$  is governed by an exact functional differential equation [6–8]

$$\partial_t \Gamma_k = \frac{1}{2} \text{Tr} \left( \Gamma_k^{(2)} + R_k \right)^{-1} \partial_t R_k. \quad (2)$$

Here, we have introduced the logarithmic flow parameter  $t = \ln(k/\Lambda)$ , and a momentum dependent regulating function  $R_k(q^2)$ , which ensures that only the fluctuations above the Wilsonian cutoff scale are being integrated out. The  $\Lambda$  is the momentum scale on which our theory was initially defined.  $\Gamma_k^{(2)}[\bar{\phi}]$  is a shorthand notation for the second functional derivative  $\delta^2 \Gamma_k / \delta \bar{\phi} \delta \bar{\phi}$ , and the trace denotes an integration over the momentum. Alternatively one can introduce a  $\bar{\rho} \equiv \frac{1}{2} \bar{\phi}^2$ , and from now on we are going to use this as our variable. Let us note that in the LPA, the two-dimensional Wegner-Houghton RG equation (i.e. the sharp cutoff regulator) is mathematically equivalent (see e.g. [11]) to the effective average action RG equation [6, 7] with the power-law regulator  $R_k(q^2) \equiv q^2 (q^2/k^2)^{-b}$  [8] with  $b = 1$  and the functional Callan-Symanzik RG equation [16]. By inserting Eq.(1) into Eq.(2) one will obtain the flow equation for the effective potential

$$\partial_t U_k = \frac{1}{2} \int \frac{d^D q}{2\pi^D} \partial_t R_k \left( \frac{N-1}{q^2 + R_k + U'_k} + \frac{1}{q^2 + R_k + U'_k + 2\bar{\rho} U''_k} \right). \quad (3)$$

This equation on the right hand side defines a loop-integral structure with the propagators of the  $N - 1$  Goldstone modes and the single massive radial mode. The integration by the momentum  $q$  can be performed by choosing the  $R_k(q^2)$  regulator function in a way it satisfies all the following requirements:  $\Gamma_k$  approaches the bare action in the limit  $k \rightarrow \Lambda$  and the full quantum effective action when  $k \rightarrow 0$  [9]. Various types of regulator functions can be chosen, but a more general choice is the so called CSS regulator [24–26] which recovers all major type of regulators in its appropriate limits. By using a particular normalisation [25, 26] and the notation  $y = q^2/k^2$ , the dimensionless CSS regulator ( $r_k(q^2) \equiv R_k(q^2)/q^2$ ) has the following form

$$r_{\text{css}}^{\text{norm}}(y) = \frac{\exp[\ln(2)c] - 1}{\exp\left[\frac{\ln(2)cy^b}{1-hy^b}\right] - 1} \theta(1 - hy^b), \quad (4)$$

with the Heaviside step function  $\theta(y)$  where the limits are

$$\lim_{c \rightarrow 0, h \rightarrow 1} r_{\text{css}}^{\text{norm}} = \left( \frac{1}{y^b} - 1 \right) \theta(1 - y^b), \quad (5a)$$

$$\lim_{c \rightarrow 0, h \rightarrow 0} r_{\text{css}}^{\text{norm}} = \frac{1}{y^b}, \quad (5b)$$

$$\lim_{c \rightarrow 1, h \rightarrow 0} r_{\text{css}}^{\text{norm}} = \frac{1}{\exp[\ln(2)y^b] - 1}. \quad (5c)$$

Thus, the CSS regulator has indeed the property to recover all major types of regulators: the Litim [10], the power-law [8] and the exponential [6] ones. Let us note, in the LPA the momentum integral of the RG equation can be performed analitically in some cases, e.g. by using the Litim, the sharp, and the  $b = 1, 2$  power-law cutoffs. By using the optimised (or Litims) regulator [10],  $R_k(q^2) = (k^2 - q^2) \theta(k^2 - q^2)$ , one can evaluate the integral in Eq.(2) analytically. In the mean time we introduce the following dimensionless variables in order to be able to extract the fixed point structure of the Wetterich equation Eq.(2):

$$\begin{aligned} u(\rho) &= U/k^D, \\ \rho &= \frac{1}{2} \bar{\phi}^2 k^{2-D}. \end{aligned} \quad (6)$$

At the end of the procedure one will obtain the flow equation for the dimensionless effective potential in  $D$  Eucledian dimensions:

$$\partial_t u = -Du + (D-2)\rho u' + (N-1) \frac{A_D}{1+u'} + \frac{A_D}{1+u'+2\rho u''}. \quad (7)$$

The first two terms arise due to the canonical dimension of the potential and of the fields, whereas the third and fourth term is a consequence of the fluctuations of the  $N-1$  Goldstone modes and the radial mode, respectively. The numerical factor  $A_D$  comes from the angular integration of the  $D$  dimensional integral in Eq.(3), and it could be absorbed by using a rescaling  $\rho \rightarrow \rho/A_D$  and  $u \rightarrow u/A_D$ , but we will choose not to do that, to show the explicit dimension dependence. ( $A_D$  can be set to 1 at any point). In the following Section we are going to study the scaling solutions of Eq.(7).

## II. THE VANISHING BETA FUNCTION CURVES

First we are assuming that we can expand the potential in a Taylor-series around vanishing field. That is:

$$u(\rho) = \lim_{n \rightarrow \infty} \sum_{i=1}^n \frac{u^{(i)}}{i!} \rho^i. \quad (8)$$

For the sake of simplicity we are going to use the following notations for the coefficients  $\lambda_i \equiv u^{(i)}(0)$ . But most of the times we are also going to use for the quadratic coupling  $\lambda_1 \equiv m^2$ , sometimes for the quartic coupling  $\lambda_2 \equiv \lambda$  and  $\lambda_3 \equiv \tau$  for the sextic coupling. Keeping this in mind we can look at the flow equation of the effective potential and differentiate it once, then evaluate it at  $\rho = 0$ . So we get the flow equation for the mass

$$\partial_t m^2 = (D-2)m^2 - Dm^2 - \frac{3\lambda A_D}{(1+m^2)^2} - \frac{(N-1)\lambda A_D}{(1+m^2)^2}. \quad (9)$$

If we are looking for the scale independent solutions (i.e. the fixed point solutions) of this partial differential equation, one can take  $\partial_t m^2 = 0$ . By doing this, we can express  $\lambda$  by using only the mass term

$$\lambda = -\frac{2m^2(1+m^2)^2}{(2+N)A_D}. \quad (10)$$

This curve defines the value of  $\lambda$ , provided  $\partial_t m^2 = 0$ , i.e. this relation is only true when the mass stopped running [22], [27]. If one does not have quartic coupling, i.e.  $\lambda = 0$ , then the solutions for this equation are just the roots of  $\lambda(m^2)$ , that is  $m^2 = -1$  or  $m^2 = 0$ . Now we derive the flow equation for the quartic coupling, too. To do so, we need to perform the same idea as before, but now we need to differentiate the flow equation of the effective potential twice respect to  $\rho$  and only then evaluate it at  $\rho = 0$ . One will have then:

$$\partial_t \lambda = 2(D-2)\lambda - D\lambda + \left( \frac{18\lambda^2}{(1+m^2)^3} - \frac{5\tau}{(1+m^2)^2} \right) A_D + (N-1) \left( \frac{2\lambda^2}{(1+m^2)^3} - \frac{\tau}{(1+m^2)^2} \right) A_D. \quad (11)$$

Again, if we are interested in the fixed point of the equation we need to take  $\partial_t \lambda = 0$ , which enables us to express the sextic coupling as  $\tau = \tau(\lambda, m^2)$ . If we are looking for the fixed points of both equations Eq.(11) and Eq.(9) we can express the sextic coupling by only using the mass as an explicit parameter:  $\tau = \tau(\lambda(m^2), m^2) = \tau(m^2)$ . This looks as follows:

$$\tau = -\frac{2m^2(1+m^2)^3(D(1+m^2)(2+N) - 4(2+N+2m^2(5+N)))}{(2+N)^2(4+N)A_D^2}. \quad (12)$$

This function defines the value of  $\tau$ , provided  $\partial_t m^2 = 0$  and  $\partial_t \lambda = 0$ . When we are looking for a fixed point for the whole system of equations we need to set the left hand side of Eq.(12) to zero (which sets  $\partial_t \tau = 0$  automatically), thus providing the values for  $m^2$  where the fixed points are found. The general statement is the following: one can express the  $n$ th coupling simply by using the mass term  $m^2$  as an explicit parameter. This nesting formula has the following form:

$$\lambda_n = \lambda_n(\lambda_{n-1}(\lambda_{n-2}(\dots \lambda_2(m^2))), m^2) = \lambda_n(m^2). \quad (13)$$

It is easy to prove it in few lines using induction. If it is so, then one can find a formula which tells the general form for the  $n$ th coupling for  $n \geq 2$ :

$$\lambda_n = (-1)^{n+1} \frac{2^{\lfloor n/2 \rfloor}}{A_D^{n-1} \prod_{i=1}^{n-1} (2i + N)^{\lfloor (n-1)/i \rfloor}} m^2 (1 + m^2)^n \sum_{i=0}^{n-2} \sum_{j=0}^{n-2} f_{i,j}(N^\alpha) (m^2)^i D^j. \quad (14)$$

Here the notation  $\lfloor \cdot \rfloor$  means the integer part of its argument and  $f_{i,j}(N)$  is an integer valued function of  $N^\alpha$ , where  $\alpha$  is an integer, too. From Eq.(14) we can conclude that (apart from the prefactor which depends only on  $N$  and  $D$ )  $\lambda_n$  is a polynomial of  $m^2$  over the integers, which has roots at  $m^2 = 0$  and  $m^2 = -1$  for every  $n \geq 2$ . Another interesting consideration is that  $\lambda_2$  is the greatest common divisor of all the  $\lambda_n$  VBF,  $n \geq 2$ . Of course there are much more roots in the complex numbers domain in general (actually the number of roots are growing with  $n$ ), but we are only going to consider the real ones (if it is not necessary to do otherwise, like in  $D = 4$ ), for which the physics is sensible. It is worth to emphasize that Eq.(14) is the most general form of the couplings  $\lambda_n(m^2)$ , their qualitative behaviour highly depend on the dimensionality, as we are going to see later on. It also depends on the number of the fields  $N$  of course but this dependence is rather quantitative.

The couplings  $\lambda_n = \lambda_n(m^2)$  in Eq.(14) defines a curve in terms of  $m^2$  on which  $\partial_t \lambda_{n-1} = 0$ , i.e. the beta function of the  $(n-1)$ th coupling, vanishes. But we know that  $\lambda_{n-1} = \lambda_{n-1}(m^2)$  (which we have already in hand, otherwise we could not build up  $\lambda_n(m^2)$ ) defines a curve on which  $\partial_t \lambda_{n-2} = 0$ , and we can continue this till  $n = 1$ . For this reason from now on we will refer to the curves defined in Eq.(14) as Vanishing Beta Function curves (VBF).

As a next step we would like to extract the fixed points of the theory. The VBF-curves of course define the possible values of the couplings for the fixed points. In order to find a fixed point we need to perform the following procedure. The VBF  $\lambda_n$  defines a curve where  $\partial_t \lambda_{n-1}$  vanishes, but it does not say anything about  $\partial_t \lambda_n$  itself. The curve which on  $\partial_t \lambda_n$  vanishes is defined by  $\lambda_{n+1} = \lambda_{n+1}(m^2)$ , and so on. But we need to cut our Taylor-expansion at some order, to be able to carry out real computations. Let us say we truncate it at the  $n$ th order, but then again we would need the beta function of  $\lambda_n$  to be zero, which is encoded in the VBF defined by  $\lambda_{n+1}$ . Since we expanded the effective potential in Taylor-series till the  $n$ th order clearly we cannot construct that curve. The only way to get  $\partial_t \lambda_n = 0$  is to set  $\lambda_n(m^2) \equiv 0$  which gives zero for its beta function automatically. In other words, assume that we would like to have an  $(n-1)$  order expansion, but before we do so we do not set  $\lambda_n = 0$  for the moment. If  $\lambda_n$  would not be zero we would need its beta function to vanish, too, in order to find a fixed point. But we do not want to compute its beta function, because at the end we are satisfied with an  $n-1$  order expansion. Since we did not set  $\lambda_n$  to zero yet we can express it through the vanishing beta function of the  $(n-1)$ th coupling because its fixed point equation has the form  $\partial_t \lambda_{n-1} = 0 = F(m^2) + \lambda_n$ , where  $F(m^2)$  is a polynomial in  $m^2$ . Now,  $\lambda_n = -F(m^2)$ , which just defines its VBF curve. Since we did not want to have this term (i.e. the  $n$ th), we can set  $F(m^2) = 0$ , which is satisfied at its roots  $m_0^2$ 's, hence  $\lambda_n = 0$ , too. Thus, although practically we expanded the effective potential till the order  $n$  and we were able to construct the VBF curves all the way till order  $n$ , we must find the roots of the  $n$ th VBF curve to set the  $n$ th coupling to zero, which would imply by construction that  $\partial_t \lambda_n \equiv 0$ . To make a long story short: we have to solve the following equation

$$\lambda_n(m_0^2) = 0. \quad (15)$$

Where  $m_0^2$  represents the roots of the VBF curve  $\lambda_n(m^2)$ . We need to evaluate the other  $n-1$  VBF curves at these  $m^2 = m_0^2$  points to obtain the value of all the dimensionless couplings at the fixed point, and thus define the truncated effective fixed point potential. So far so good, but let us suppose we find a fixed point potential which is unbounded from below, i.e. defines an instable theory. That obviously must be wrong, hence we need to bring into play another restriction: since the potential is a polynomial, the asymptotics (i.e. the boundedness from below for large field values) depend on the highest degree term in the polynomial. As a consequence we need to exclude the  $m_0^2$  roots that give  $\lambda_{n-1}(m_0^2) < 0$  coupling, which is the coefficient of the highest degree nonzero term in the polynomial expansion.

In general we can sum up all these requirements in the following way. Let us define the set  $M = \{m_0^2 \in \mathbb{R} | \lambda_n(m_0^2) = 0\}$ . A stable fixed point effective potential can be found by substituting all  $m_0^2 \in M$  into the  $n-1$  VBF curves  $\{\lambda_{n-1}(m^2)\lambda_{n-2}(m^2), \dots, \lambda_2(m^2), \lambda_1 \equiv m^2\}$  provided  $\lambda_{n-1}(m_0^2) \geq 0$ . (If it happens to be zero, too, one need to apply this rule for the VBF  $\lambda_{n-2}(m^2)$ , and so on). In other words the set of  $m_0^2$ 's which defines a true fixed point is

$$M^* = \{m_0^2 \in \mathbb{R} | \lambda_n(m_0^2) = 0 \wedge \lambda_{n-1}(m_0^2) \geq 0\}. \quad (16)$$

In the following, some example are presented individually for  $D \leq 2$ ,  $2 < D < 4$  and  $D \geq 4$ , starting with  $D \leq 2$ .

### III. VBF CURVES FOR $D \leq 2$ $O(N)$ THEORIES

#### A. Continuous symmetries ( $N \geq 2$ )

The Mermin-Wagner theorem essentially states that no spontaneous breaking of continuous symmetry is present in systems of  $D \leq 2$ . In [23] a numerical evidence was given in the framework of the FRG that the MW indeed holds, here beyond LPA scheme was used. It was recently shown in [22] using analytical considerations that even at the LPA level the MW is not violated, provided a non-expanded treatment of the effective potential. There has been argued that if the potential is Taylor-expanded, then the restoration of the Mermin-Wagner theorem can be seen at large enough expansion. We will verify this statement by applying the rules that have been settled above.

Using Eq.(14) for  $D = 1$  and  $D = 2$  case one can find a simplified expression for the  $n$ th coupling

$$\lambda_n \propto (-1)^{n+1} m^2 (1 + m^2)^n \sum_{i=0}^{n-2} g_i(N, D) (m^2)^i. \quad (17)$$

Here we only indicated the polynomial structure in  $m^2$ , although the prefactors are slightly modified, too. The coefficient functions  $g_i(N, D)$  are defined as follows:

$$g_i(N, D) = \sum_{j=0}^{n-2} f_{i,j}(N^\alpha) D^j. \quad (18)$$

Interestingly, setting  $D \leq 2$  will imply that all the  $g_i$ s are positive for every term. This fact suggests that the roots (which are not complex) must be either negative or zero.

Let us find the fixed points according to the rule that has been established in the previous section, using  $N = 3$  and  $D = 2$ . The following VBF curves are found to be:

$$\begin{aligned} \lambda_2 &= -\frac{8\pi}{5} m^2 (1 + m^2)^2, \\ \lambda_3 &= \frac{64\pi^2}{175} m^2 (1 + m^2)^3 (5 + 27m^2), \\ \lambda_4 &= -\frac{512\pi^3}{7875} m^2 (1 + m^2)^4 (25 + 670m^2 + 1671(m^2)^2), \\ \lambda_5 &= \frac{4096\pi^4}{606375} m^2 (1 + m^2)^5 (175 + 18595m^2 + 161115(m^2)^2 + 254799(m^2)^3), \\ &\dots \end{aligned} \quad (19)$$

Considering only the real roots, we can find that they are all situated in the interval  $[-1, 0]$ . On Fig.(1), one can see the plot of the VBF curves versus  $m^2$ . The mere fact that we can find roots is against the Mermin-Wagner theorem, for which to find it being true, we should have no roots at all, except at the ending points of the interval  $[-1, 0]$ . We found true fixed point potentials at a finite truncation level according to Fig.(1) which should not be there as a consequence of to the MW theorem. The situation is getting worse when we go to higher order in the truncation: indeed, in this case we are going to have more zeros, hence more and more fixed point potentials emerge. How can we resolve this contradiction? One way would be to overcome this situation is that all the roots between  $-1$  and  $0$  turn into complex valued as we go to higher order. However, from the order of the expansion we used we cannot put our hope in this. There is another scenario, too. Let us analyse the VBF curves more carefully. Apparently, one can find a pattern of the roots for the VBF curves: evaluating the  $\lambda_{n-1}$  VBF at each of these roots of  $\lambda_{n-1}$  one will find real numbers alternating in sign starting from the closest root to  $-1$  with  $\text{sgn} \lambda(m_1^2) = +1$  (here the 1 in the subscript indicates the closest root to -1). For instance in our example on Fig.(1) that was  $m_0^2 = -0.484$  corresponding to the stable potential (Fig.(3)). In other words from the set  $M$  we defined above we will consider only  $M \setminus \{-1, 0\}$  and the claim is: if we make an ordering from the smallest value to the largest in this set then every odd element of  $M \setminus \{-1, 0\}$  is in the set of  $M^* \setminus \{-1, 0\}$ , hence for every such element  $\lambda_{n-1} > 0$  thus defining a stable potential. So, we are still going to have fixed points even though the number of them is halved by taking into account only the fixed points which define stable potential. It seems it did not help a lot but actually from this information we can extract some useful information: each root of the  $\lambda_n$  VBF are surrounded by the roots of the  $\lambda_{n-1}$ , otherwise the alternating signs that was explained above could not be possible. So, it means that by deriving higher and higher order VBF curves the position and the number of roots change in the way that all of the old roots are around the new ones, see Fig.(2). Let us call this interesting pattern  $M^*$  pattern for future use. We can do one thing with this

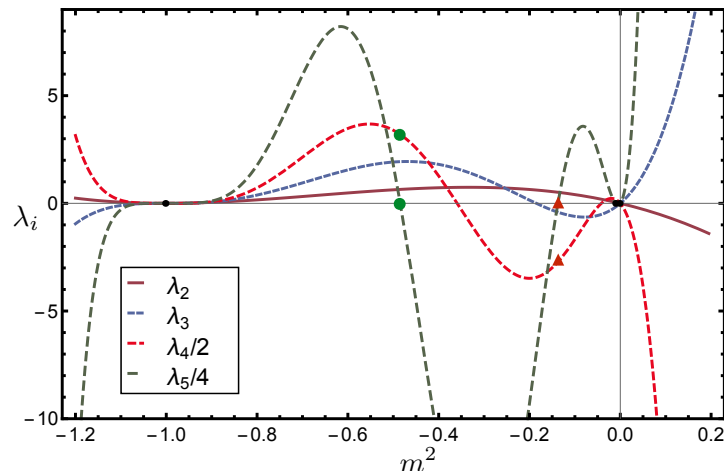


FIG. 1: The VBF curves for the couplings  $\lambda_2, \lambda_3, \lambda_4$  and  $\lambda_5$ . Each curve is defined by the vanishing beta functions:  $\partial_t m^2 = \partial_t \lambda_2 = \partial_t \lambda_3 = \partial_t \lambda_4 = 0$  respectively. The roots for  $\lambda_5(m^2)$  is indicated by black dots. These roots are going to define the fixed point potentials at the truncation level  $n = 4$ . Two roots are distinguished and being indicated by a green dot and red triangle to demonstrate a valid and a false fixed point. At the green dot ( $m^2 = -0.484$ ) we find that  $\lambda_4 > 0$ , and evaluating  $\lambda_4$  at the red triangle ( $m^2 = -0.137$ ) we get  $\lambda_4 < 0$ , hence defining an unbounded potential, See Fig.(3). On  $\lambda_4$  and  $\lambda_5$  a scaling is performed because of display purposes.

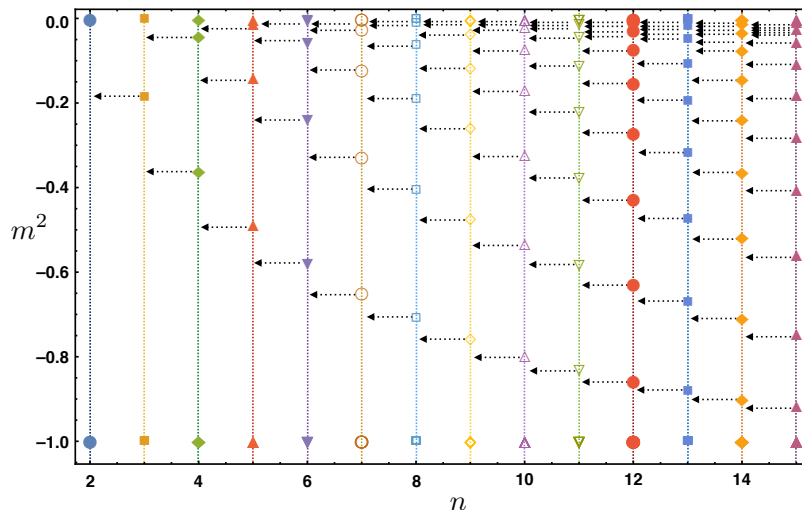


FIG. 2: The roots of the VBF curves  $\lambda_2, \dots, \lambda_{15}$ . Observe the pattern which is given by the following rule: any root of  $\lambda_n$  is between the roots of  $\lambda_{n-1}$  (except for  $-1$  and  $0$  of course).

without knowing anything about the structure but the root pattern statistics: we can simulate a sequence of sets of points which behave in this way.

Let us consider a randomly generated number  $X_1$  which can take a value in the interval  $(-1, 0)$ . We generate this number and then we consider two new random numbers  $X_2^1$  and  $X_2^2$ . The first one can take any value in the interval  $(-1, X_1)$  and the second in  $(X_1, 0)$ . After we generate values for  $X_2^1$  and  $X_2^2$  they are going to be the new ending points of the intervals where we define again random numbers but this time three:  $X_3^1, X_3^2$  and  $X_3^3$ . We continue this procedure with the random numbers  $X_n^i$  with  $i = 1, 2, \dots, n$  and  $n \rightarrow \infty$ , where  $n$  indicates that we define them in the  $n$ th step in the interval  $(X_{n-1}^1, X_{n-1}^n)$ , including  $-1$  and  $0$ , too. By increasing  $n$  we can obtain the distribution of the points created in the way described above Fig.(4). From this construction one can see that the distribution of the

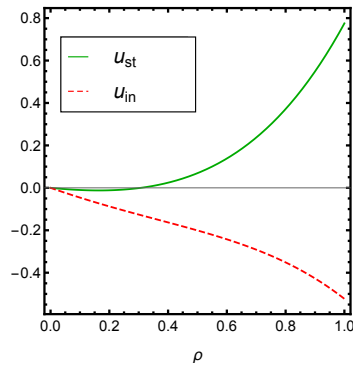


FIG. 3: The fixed point potentials evaluated at the fixed point discussed in Fig.(1). A stable potential can be obtained for  $m^2 = -0.484$  and an instable one for  $m^2 = -0.137$ , which are indicated on the figure by  $u_{st}$ ,  $u_{in}$ , respectively.

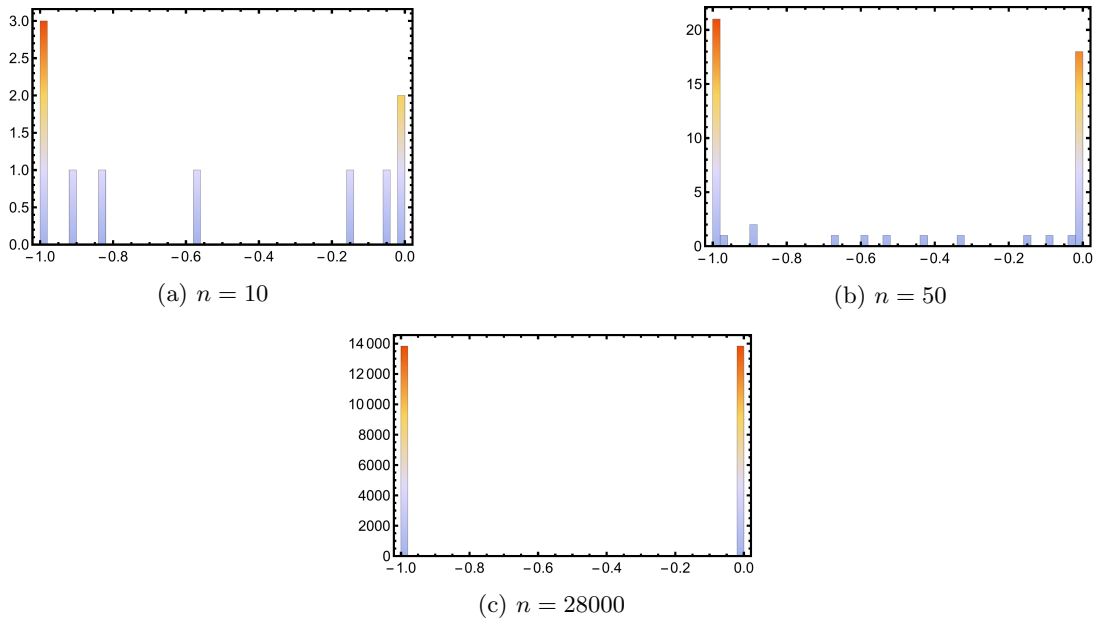


FIG. 4: Histograms of the distribution of the points generated in  $X_n$ . On the subfigure (a) the distribution of  $X_{10}$  on the subfigure (b) the distribution of  $X_{50}$  and on the subfigure (c) the distribution of  $X_{28000}$  are displayed. Note that the positions of the points are tending to  $-1$  and  $0$  and at very high  $n$  the number of points between the two endpoints is negligible, in other words: the probability of finding a point between the two endpoints is tending to zero as  $n \rightarrow \infty$ .

randomly generated points is changing in a way that they are accumulating at the two ending points of the interval. This suggests that the limit of the probability density for  $X_n$  is (at least in distributional sense):

$$\lim_{n \rightarrow \infty} f_{X_n}(x) = \frac{1}{2}(\delta(x+1) + \delta(x)). \quad (20)$$

The aim was to simulate the zeros of the VBF polynomials  $\lambda_n$ , and we found that the roots are accumulating at  $-1$  and  $0$ . Thus, if there exist a limit for the VBFs ( $\lim_{n \rightarrow \infty} \lambda_n = \lambda$ ), then this will give zero only at  $-1$  and  $0$  even if this limit is not a continuous function. But this is physically well-justified since this would indicate that we do not find any roots other than the two ending points of the interval, which leads us to the conclusion that no SSB is present in dimensions  $D = 2$  with  $N = 3$ . Indeed, this is a seemingly paradoxical result, namely that we would expect infinitely many number of fixed points as the degree of the VBF polynomials grow, but at the end we will find two actual fixed points defining only one phase, in agreement with the Mermin-Wagner theorem that we wanted to show.

We can make another remark on the role of the convexity fixed point  $m^2 = -1$ . From the VBFs one can see that every higher coupling vanishes at this point, i.e.  $\lambda_2(-1) = \lambda_3(-1) = \dots = 0$ , hence the potential which is defined by

this fixed point is an unstable one. One can now speculate whether this fixed point is a real one or it is just an artefact of the approximations that we use in the FRG. However, we can make another note on this. We identified the pattern for the fixed points by considering the roots of the VBFs in the open interval  $(-1, 0)$ , and it is in growing order: the first is a well defined the second is not the third defines a stable potential again, and so on. What would we get if we extended this pattern to the closed interval  $[-1, 0]$  and we would consider only the limit of the VBFs which has two zeros, according to the root pattern statistics, situated exactly at the ending points? The Gaussian ( $m^2 = 0$ ) would always give a well defined non-interacting potential and there is no chance for  $m^2 = -1$  to be well defined according to the  $M^*$  pattern.

Similar results can be obtained both for the  $D = 1$  (see Fig.(5)). For  $N$  dependence and fractional dimensions see Section VI and VII, respectively.

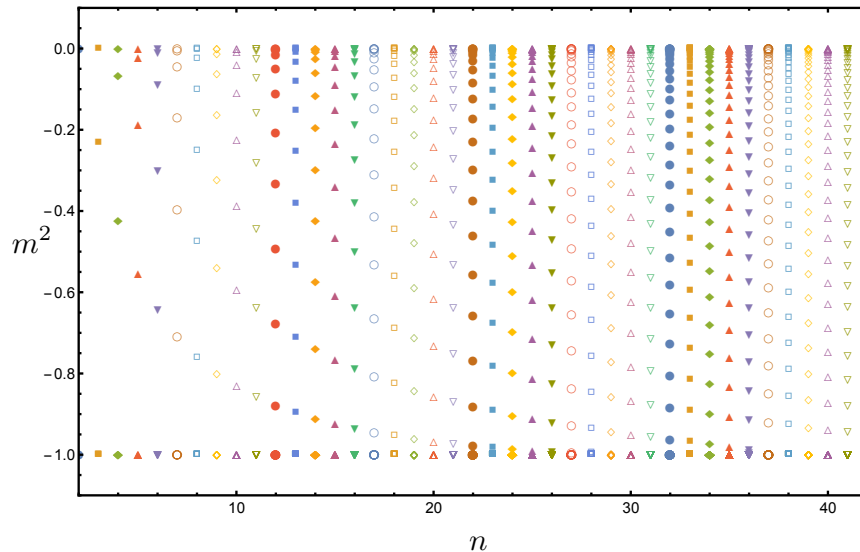


FIG. 5: Roots of a  $D = 1$  dimensional theory with  $N = 3$  field components. A similar structure can be observed as on Fig.(2).

### B. $\mathbb{Z}_2$ symmetry ( $N = 1$ )

In the case of the discrete symmetry the  $O(N)$  theory is equivalent to the Ising model, and as the symmetry is being non continuous the MW theorem does not necessarily hold for  $N = 1$ . Indeed, it is well known that in the Ising model we can find a spontaneous symmetry breaking even in the  $D = 2$  case, which was carried out in an exact calculation by Onsager [21]. Here, we are going to see that we can reproduce this result using the technique introduced above.

On Fig.(6) we can see the position of the roots for  $D = 1$  and 2 with  $N = 1$  on a separate plot. The VBF polynomials are described by Eq. (17) with different  $g_i$  coefficients of course. We can see qualitative difference between the two figures, namely, in the one dimensional case, the first root is converging to  $m^2 = -1$  and for the two dimensional the asymptotic goes to  $m^2 = -0.835$  defining a threshold for all the roots in higher orders. One can fit a function of the form of  $f(x) = a + bx^c$  on the positions of the first roots, with fit parameters  $a = -1.00 \pm 0.0002$ ,  $b = 2.08 \pm 0.002$  and  $c = 0.85 \pm 0.0006$  in  $D = 1$ ,  $a = -0.835 \pm 0.001$ ,  $b = 1.56 \pm 0.004$  and  $c = 0.738 \pm 0.003$  in  $D = 2$ . Now, since the root position pattern is the same as we observed above, we can apply the random number procedure for  $D = 1$  in the interval  $[-1, 0]$  and for  $D = 2$  in the interval  $[-0.835, 0]$ . The limiting result is the following: in one dimension the roots are accumulating at  $m^2 = -1$  and  $m^2 = 0$  thus we can conclude only the stable Gaussian fixed point potential is well defined at the latter. In the case of the two dimensions we will find two fixed points the Gaussian ( $m^2 = 0$ ) and another one which is at  $m^2 = -0.835$ . Now, it is a question if this fixed point is stable or not. The finding is the following: for every truncation in the present computation  $\lambda_n(m^2 = -0.835) > 0$  where the highest order was  $n = 45$ , thus we can safely state that it defines a stable fixed point potential, hence indicating a spontaneous symmetry breaking phase. It is interesting that even at LPA level one can observe the SSB for the two dimensional



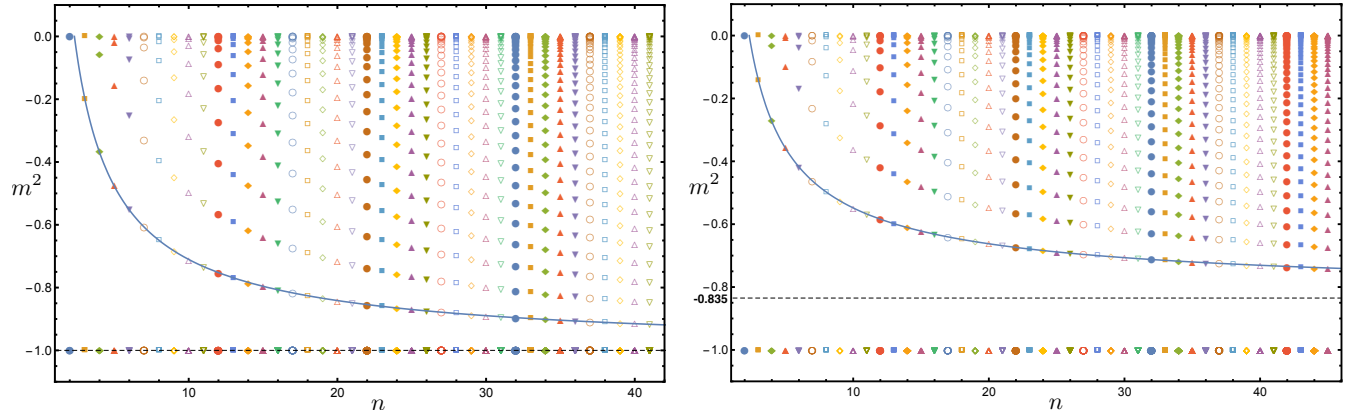


FIG. 6: On the left (right) panel the position of the roots of the VBF curves are shown for  $N = 1$  in  $D = 1$  ( $D = 2$ ). In the one dimensional case one finds the same pattern that was shown above for  $N = 3$  with a convergence to  $m^2 = -1$ . In two dimensions the roots are converging towards  $m^2 = -0.835$  signalling an SSB phase.

Ising model contrary to the finding in [22] where even with the exact spike plot technique it is undetectable, due to its dependence on the numerical precision.

#### IV. VBF CURVES FOR $2 < D < 4$ $O(N)$ THEORIES

The  $O(N)$  theories which belong to the class  $2 < D < 4$  have the richest fixed point structure, hence to study them is the most difficult. We are going to perform a detailed analysis for the only integer dimension found in this interval,  $D = 3$  specified ourselves for  $N = 2$ . We expect here to obtain the well known Wilson-Fisher fixed point in the broken regime, however we are going to see that there is no clear root structure to be observed for the roots  $m^2 > 0$ . In this case we have the following generic form for the VBFs in  $2 < D < 4$ , similarly to the Eq.(17)

$$\lambda_n \propto (-1)^{n+1} (m^2)^{1+\Theta(n-4)} (1+m^2)^n \sum_{i=0}^{n-2} g_i(N, D) (m^2)^{i-\Theta(n-4)}. \quad (21)$$

Here  $g_i(N, D)$  is defined in a similar way as above in Eq.(18), but now as we can see the exponent of  $m^2$  has changed, hence in the sum Eq. (18) there must be  $D^{\alpha(j)}$  rather than  $D^j$ , where  $\alpha(j)$  represents the exponents which were not factored out to the exponent of  $m^2$ . The function in the exponent is just the Heaviside step function  $\Theta(n-4) = 1$  if  $n \geq 4$  and 0 otherwise. Some sample from the VBFs for  $D = 3$  and  $N = 2$ :

$$\begin{aligned} \lambda_2 &= -3\pi^2 m^2 (m^2 + 1)^2, \\ \lambda_3 &= 3\pi^4 m^2 (m^2 + 1)^3 (11m^2 + 1), \\ \lambda_4 &= -27\pi^6 (m^2)^2 (m^2 + 1)^4 (23m^2 + 4), \\ \lambda_5 &= \frac{27\pi^8}{5} (m^2)^2 (m^2 + 1)^5 (2993(m^2)^2 + 719m^2 + 14), \\ \lambda_6 &= -\frac{27\pi^{10}}{5} (m^2)^2 (m^2 + 1)^6 (97167(m^2)^3 + 27418(m^2)^2 + 997m^2 - 14), \\ &\dots \end{aligned} \quad (22)$$

Contrary to the cases for  $D \leq 2$ ,  $g_i$  coefficients now can take negative values, too. From these considerations one can already expect a different root structure from that we had above. On Fig.(7) we see the VBF curves up to  $\lambda_6(m^2)$  and on Fig.(8) the root structure up to order  $n = 41$ . For our analysis we are going to separate the real line of  $m^2$  into three regions. First we will consider the roots in the interval  $[-1, 0]$ , then we will turn to the complement set separately for each disjoint intervals  $(-\infty, -1)$  and  $(0, \infty)$ . From Fig.(10) it is clear, that in the interval  $[-1, 0]$  we have a very similar pattern for the roots (after some  $n$ ) that we had in the two dimensional case. However, there is a

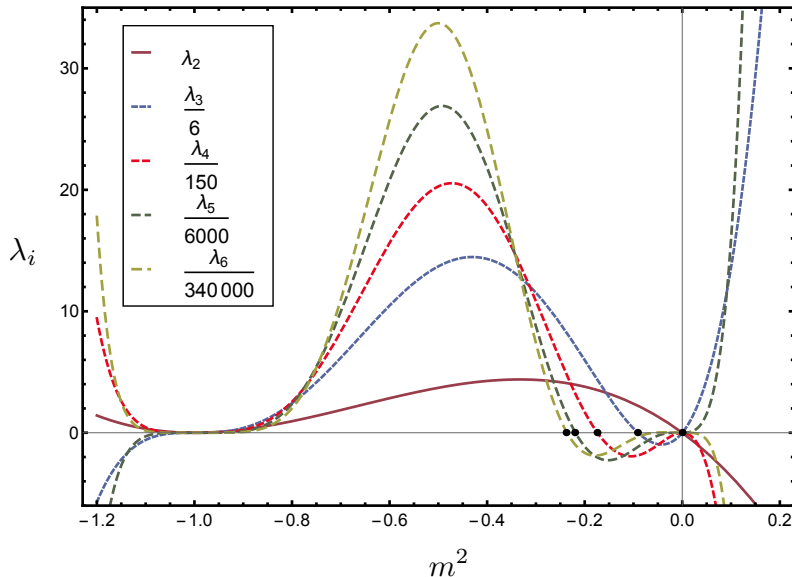


FIG. 7: On this plot the VBFs up to  $\lambda_6$  are shown for  $D = 3$ ,  $N = 2$ . Also the for each  $\lambda_i$  the root that is closest to  $-1$  (from above) is indicated with a black point. Note that the if we consider the position of these points as a sequence then it will converge to a finite value  $m^2 = -0.23$ , also see on Fig.(10).

striking difference between the  $D \leq 2$  case and the present  $D = 3$  theory: the roots are seemed to be accumulating at an  $m^2 \approx -0.23$  value rather than  $-1$ . If one restricts the pattern to the  $[-0.23, 0]$  interval, the random number generating model for the root pattern statistics becomes available again. Since the distribution of the points signals the accumulation at  $m^2 = 0$  and  $m^2 = -0.23$  the probability density for finding a root in this interval will have the same form as Eq.(20), the only difference is that the Dirac-deltas now centred at  $m^2 = -0.23$  and  $m^2 = 0$  rather than  $m^2 = -1$  and  $m^2 = 0$ . We can also check the convergence of the roots by establish an ordering among them:  $m_1^2$ ,  $m_2^2$  and  $m_3^2$ , where the first indicates the root that is the closest, the second is the second closest and the third is the third closest root to  $-1$  at each order. The root labelled by  $m_1^2$  starts to go towards  $-1$  but at order  $n = 6$  it stops and starts to converge to  $m^2 = -0.23$  in an oscillatory way. On the other hand the roots  $m_2^2$ ,  $m_3^2$  also converge to this value, and it is possible to fit a curve on them but this time the fit is an exponentially decaying one as it can be seen on Fig.(10a). The convergence of these roots confirms what we expect from the  $M^*$  pattern: the two roots that will remain in this interval is  $m^2 = 0$  and  $m^2 = -0.23$ , which correspond to the Gaussian and the Wilson-Fisher fixed point, respectively. One needs to check if the WF fixed point defines a bounded potential. Substituting the value  $m^2 = -0.23$  into the VBF polynomials  $\lambda_n$  will give the following result: there are VBF curves for which  $\lambda_n(m^2 = -0.23) < 0$  and  $\lambda_n(m^2 = -0.23) > 0$ . This is due to the oscillatory behaviour of the root  $m_1^2$ , but we know this will converge to a finite value and finally the WF fixed point can be defined as the limit of  $m_1^2$ . But until that we will find situation which would give a result that the Wilson-Fisher fixed point defines an unbounded potential from below, hence strictly speaking we should not consider it as a real fixed point. This is the case for example  $\lambda_8$  and  $\lambda_9$  (see Fig.(9)), hence this tells us that there is no Wilson-Fisher fixed point at the truncation level  $n = 8$ . Even though it is true we must not forget that the Taylor expansion is an approximation so the real fixed point structure of the theory will be found when  $n \rightarrow \infty$ , hence the "absence" of the WF fixed point can be considered as an artefact of the expansion. Let us consider now the region  $m^2 < -1$ . A magnified picture of it can be seen in Fig.(10b). Here we can observe roots which are running into the convexity fixed point as  $n$  grows. The position of the roots would show similar pattern to the  $M^*$  pattern, however here we have difficulty with the unbounded interval  $(-\infty, -1]$ . We will show how can we overcome such situation in the next section, however, there will be some requirements which are not fulfilled in the present case, we will come back to this later on. Here we can only assume that all such roots will converge to  $m^2 = -1$  providing us the IR fixed point in the  $n \rightarrow \infty$  limit. For two such of root we could give a fit of the convergence. Interestingly in this case the roots are following a different trend to approach  $-1$ : the first one is an exponential function  $f(x) = a + ce^{b(x-12)}$  with  $a = -1.014 \pm 0.005$ ,  $b = -0.39 \pm 0.01$  and  $c = -1.43 \pm 0.05$ , the second is power law  $g(x) = a + c(x - 20)^b$  with  $a = -0.885 \pm 0.003$ ,  $b = 1.35 \pm 0.08$  and  $c = -7.2 \pm 0.06$ . Neither of them goes to  $-1$  precisely, however, these were the best fits that could be found. For large  $n$  values, when these roots are very close to  $-1$ , they develop an imaginary part, hence they cannot be considered as true fixed points strictly

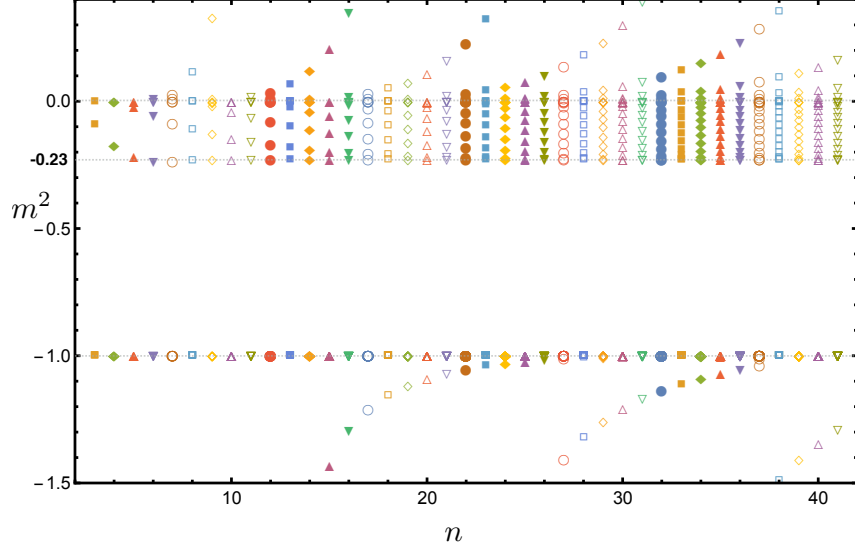


FIG. 8: Here we present the root structure of the VBF curves up to order  $n = 41$ . Observe that we can distinguish three regions where the roots are positioned:  $m^2 > 0$ ,  $m^2 < -1$  and  $m^2 \in [-1, 0]$ . For detailed picture see Fig.(10).

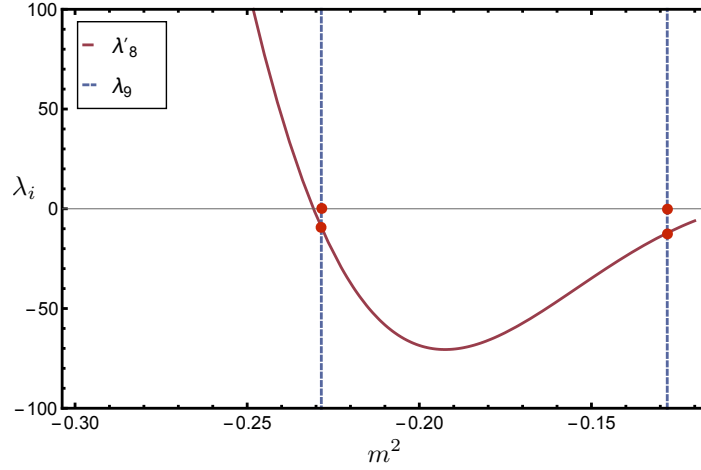


FIG. 9: The absence of the Wilson-Fisher fixed point at the truncation  $n = 8$ . We can see that the root of  $\lambda_9$  to the left define a negative valued  $\lambda(m_{WF}^2)$ , which will provide an unphysical potential at the truncation level  $n = 8$ . Moreover, the second root to the right does not give a sensible potential, too. This phenomenon occurs because of the oscillatory nature of  $m_1^2$ , at  $n \rightarrow \infty$  we would expect to see a stable fixed point potential at the WF fixed point.  $\lambda_8$  has been rescaled with a factor of  $2 \times 10^{-7}$ .

speaking. One has to go so close to  $-1$  that this fact can be considered as negligible, taking into account that the VBF curves around  $-1$  are extremely flat thanks to the  $(1 + m^2)^n$  factor in Eq.(14). Thus finding roots around  $-1$  is not always a reliable thing, it might be depend on the precision of the root finding algorithm.

The remaining region that we need to consider is the half interval  $m^2 > 0$ . A position of the roots for this region is shown on Fig.(10c). One can find again some pattern which could remind us to the  $M^*$  pattern, however in this case beside the interval is unbounded, the roots do not have a clear bound even from below. The general behaviour of the root positions that they have the last real root at about  $m^2 = 0.01 - 0.02$  (indicated by the red lane on the Fig.(10c)), and below they will have complex values. The  $M^*$  would hold for the higher roots, but we cannot state anything for sure in this region for  $n \rightarrow \infty$ . Even considering the generated complex roots does not help us to understand this

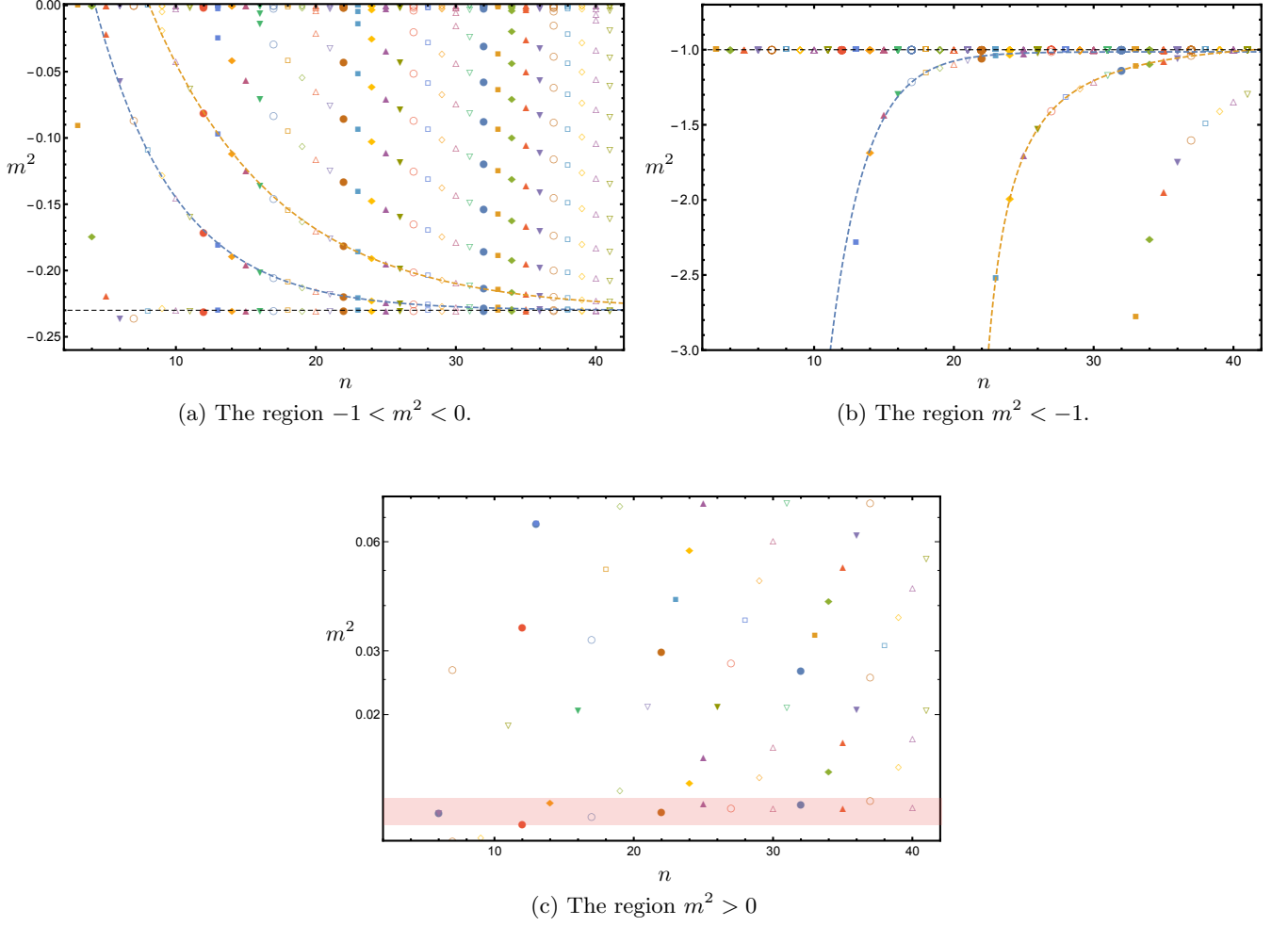


FIG. 10: The root structure of the  $D = 3$ ,  $N = 2$  theory separated to different regions. On fig (a) and (b) we can conclude for the  $n \rightarrow \infty$  limit, that is we will have the following fixed points: Gaussian, Wilson-Fisher and the IR. These suggestions are also confirmed with fitted functions. Regarding (c) for  $m^2 > 0$  no clear answer is found: the red lane indicates the last real root for  $m^2 > 0$ .

part of the root structure, but it helps in the case for the  $D = 4$  theories as we will see. The most important result of this section is the appearance of the Wilson-Fisher fixed point. It is indeed possible to find more fixed points in other fractal dimension between two and four dimensions and in different  $N$  but it is beyond the scope of the present paper.

### V. VBF CURVES FOR $D \geq 4$ $O(N)$ THEORIES

So far we considered  $D = 1, 2$  and  $3$ . In this section we are going to investigate the theories in  $D \geq 4$ . Let us look at the first two VBF curves ( $\lambda_2$  and  $\lambda_3$ ) in arbitrary dimensions and for general  $N$ . We already derived their formula in Section II: Eq.(10) and Eq.(12). Now we are interested in the zeros of the general expressions:

$$\begin{aligned}
 0 &= -\frac{2m^2(1+m^2)^2}{(2+n)A_D}, \\
 0 &= -\frac{2m^2(1+m^2)^3(D(1+m^2)(2+N) - 4(2+N+2m^2(5+N)))}{(2+N)^2(4+N)A_D^2}
 \end{aligned} \tag{23}$$

for  $\lambda_2$  and  $\lambda_3$ , respectively. The first equation gives zero at  $m^2 = -1$  and  $m^2 = 0$  independently from the dimension. Among the roots of the second equation in Eq.(23) of course we discover again  $m^2 = -1$  and  $m^2 = 0$ , but factorising with them one will be left with the equation for the third root, and it will depend on  $D$ . Let us solve it for  $m^2$ . The result is the following:

$$m^2 = \frac{-DN - 2D + 4N + 8}{DN + 2D - 8N - 40} \quad (24)$$

This expression shows us the "running" of the root (the Wilson-Fisher fixed point) in the dimension. For substituting

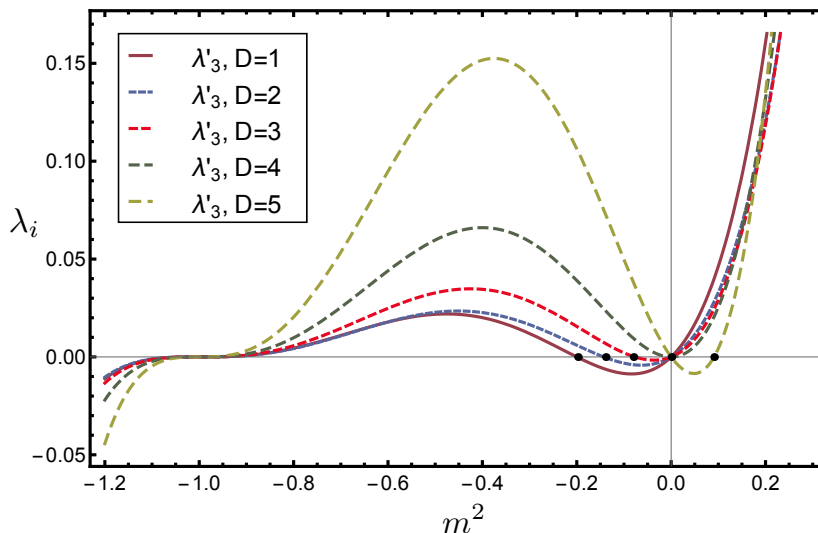


FIG. 11: On this figure one can see how the  $\lambda_3$  VBF curves change with the dimension. Observe that the only root from the  $(-1, 0)$  interval runs into zero as  $D \rightarrow 4$ . For  $D \geq 4$  the root obtain a value  $m_0^2 > 0$ , hence there is no fixed point in the SSB phase but there is one in the symmetric phase, which turns out to be unstable because  $\lambda_2(m_0^2) < 0$ .

Note that, we indicated only integer values for  $D$  but the transformation is continuous in the dimension, hence all the values between the integers would define similar curves. For this illustration  $N$  was set to 3 and the VBF curves are rescaled as:  $\lambda'_3 \propto \lambda_3 10^{-\alpha}$ , where  $\alpha = 0, 4, 4, 5$  and 6 for  $D = 1, 2, 3, 4$  and 5, respectively.

$D = 1, 2$  and 3 (and  $N = 3$ ), one would get the results that we obtained in the previous sections. However, evaluating it at  $D = 4$ , we will loose the  $N$  dependence completely. In other words: no matter what  $O(N)$  theory we consider, the WF fixed point coincides with the Gaussian in the  $D = 4$  case. On Fig.(11) one can see the  $\lambda_3$  VBF for various dimensions. The observation is the following: the only root in the interval  $(-1, 0)$  drifts towards the positive real values. At  $D = 4$  it merges into zero, hence besides the convexity and the Gaussian fixed point there are no further fixed points present. Above four dimensions the root gets positive values. We can address the question if this is a true fixed point or not. If one substitutes the value of these positive roots into the VBF  $\lambda_2(m^2)$  one will immediately see that  $\lambda_2(m_0^2) < 0$  defines an unstable potential at this truncation level, thus there is no any other true fixed points besides the Gaussian and the IR, hence we can call the system trivial. It is possible to derive the dimension dependence for other  $\lambda_i$ s, too, with similar qualitative behaviour: the roots start from inside the interval  $(-1, 0)$  with  $D = 1$  and as the dimension grows, they are tending out from the interval. As  $D$  takes the value of 4, the last (i.e. the closest to  $m^2 = -1$ ) root of the VBF under consideration merges into  $m^2 = 0$ , and all the others have already obtained positive values, see Fig.(12), where we illustrate this situation with  $\lambda_4$ . In the following we are going to discuss the VBF curves on a higher truncation level for  $D = 5$  in details as a representative of theories for  $D > 4$ . However, we need to distinguish the  $D = 4$  cases since showing the triviality for them is not that self explanatory as it is for  $D > 4$ , hence the four dimensional case is going to be presented in a separate subsection. In the last two sections various examples for theories in dimension  $D \geq 4$  are shown.

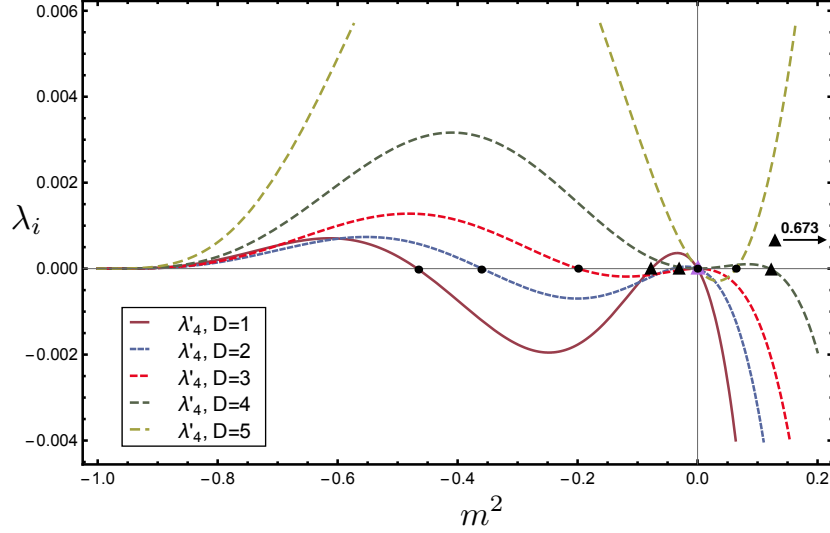


FIG. 12: On this figure one can see the different  $\lambda_4$  VBF curves for different dimensions. Observe that the two roots from the interval  $(-1, 0)$  runs to the right as  $D$  grows. For  $D = 4$  the root indicated with triangle has already a positive value and the one which was indicated by a dot has just melted into zero. For  $D = 5$  both of the roots have positive value, the triangle is not on the plot, since it took the value  $m^2 = 0.673$ . For this illustration  $N$  was set to 3 and the VBF curves are rescaled as:  $\lambda'_4 \propto \lambda_4 10^{-\alpha}$ , where  $\alpha = 5, 6, 7, 8$  and  $9$  for  $D = 1, 2, 3, 4$  and  $5$ , respectively.

#### A. Triviality for $O(N)$ theories in $D > 4$

The finding is that for any  $D > 4$  theories the VBF curves has similar structure:

$$\lambda_n \propto (-1)^{n+1} (m^2) (1 + m^2)^n \sum_{i=0}^{n-2} g_i(N, D) (m^2)^i. \quad (25)$$

Notice that it has essentially the same structure that we had in the cases  $D \leq 2$ , but there is one crucial difference. For theories  $D \leq 2$  we found the coefficient functions  $g_i$ s to be always positive, hence defining only negative (and complex) roots for the polynomial moreover they were inside the interval  $[-1, 0]$ . In this case likewise to  $2 < D < 4$  we can obtain negative values for  $g_i$ s, too, but contrary, here we do not obtain roots inside the interval  $(-1, 0)$ : all the real roots in this case positioned in the disjoint union of the complement of  $(-1, 0)$ , i.e. in  $(-\infty, -1] \cup [0, \infty)$ . The first few VBFs are the following:

$$\begin{aligned} \lambda_2 &= -24\pi^3 m^2 (m^2 + 1)^2, \\ \lambda_3 &= \frac{288\pi^6}{7} m^2 (m^2 + 1)^3 (39m^2 - 5), \\ \lambda_4 &= -\frac{1536\pi^9}{7} m^2 (m^2 + 1)^4 (576(m^2)^2 - 425m^2 + 25), \\ \lambda_5 &= \frac{92160\pi^{12}}{539} m^2 (m^2 + 1)^5 (10233(m^2)^3 - 176625(m^2)^2 + 36125m^2 - 1225), \\ &\dots \end{aligned} \quad (26)$$

These curves are being shown on Fig.(13). Now we are going to analyse their root structure. In the case for theories  $D > 4$  we can clearly identify a pattern of the roots again, just like we did it for  $D \leq 2$ , i.e. the  $M^*$  pattern. For the particular case  $D = 5, N = 3$  one can see the position of the VBF roots on Fig.(14). What we can observe it is just the inside-out situation that happened in the theories for  $D \leq 2$ . The roots are situated only outside the interval  $(-1, 0)$  and they have a similar pattern that we had for the  $D \leq 2$  cases, i. e. each root of  $\lambda_{n+1}$  is surrounded by the roots of  $\lambda_n$ . We can call it only similar since we clearly have a problem in the present case: we are not able to

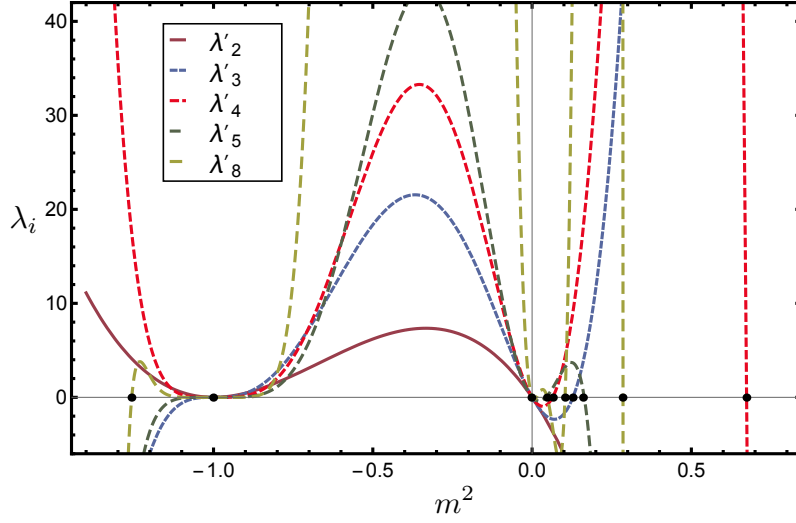


FIG. 13: The VBF curves  $\lambda'_i$  ( $i=2,\dots,5,8$ ). Observe that the roots of each curve are always outside the interval  $(-1, 0)$ . For  $\lambda_8$  we have negative roots, too. For display purposes the VBF curves are rescaled as:  $\lambda'_i \propto \lambda_i 10^{-\alpha}$ , where  $\alpha = 1, 3, 6, 9$  and  $19$  for  $i = 2, 3, 4, 5$  and  $8$ , respectively.

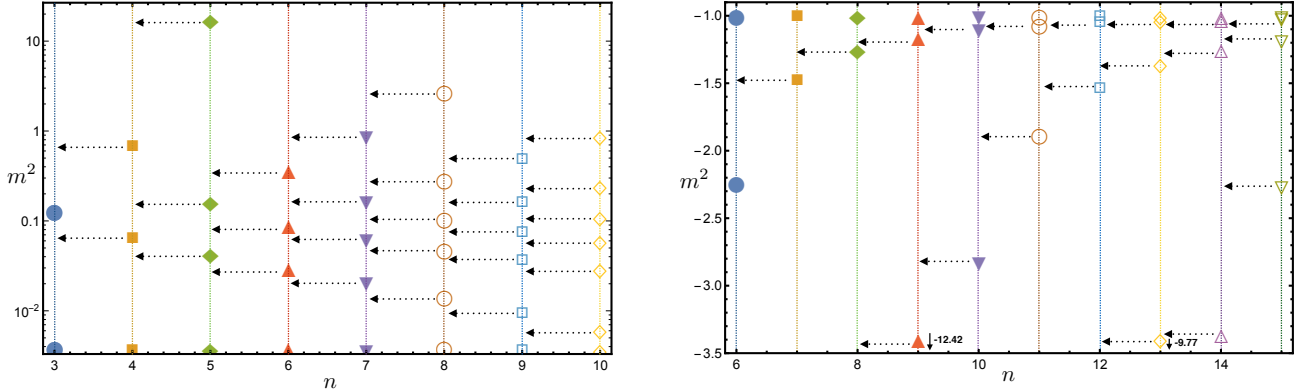


FIG. 14: On the left (right) panel the roots of the VBF curves are shown for  $\lambda_3, \dots, \lambda_{10}$  ( $\lambda_6, \dots, \lambda_{15}$ ), for  $m^2 \geq 0$  ( $m^2 \leq -1$ ). One can observe a pattern of the roots similar to the  $D \leq 2$  case: each root of VBF  $\lambda_{n+1}$  is surrounded by the roots of  $\lambda_n$ . The only problem in this case is, since the interval is unbounded, this pattern is not entirely true: indeed, the highest (lowest) roots of  $\lambda_{n+1}$  now do not have an upper (lower) neighbour from the roots of  $\lambda_n$ . We can overcome this difficulty by one-point compactifying the real line  $\mathbb{R}$ . For details see the text.

use our random number generating model that we did in Section III for simulating the positions of the roots, because the set  $(-\infty, -1] \cup [0, \infty)$  is unbounded. For that reason, the highest (lowest) roots of the VBF  $\lambda_{n+1}$  do not have an upper (lower) neighbour from the set of the roots of the VBF  $\lambda_n$ . However, we are able to do the following trick: let us one-point compactify the real line  $\mathbb{R}$ , meaning that we “glue” together the points  $m^2 \rightarrow \pm\infty$ , thus creating a closed set for  $[0, -1]$ . This may look an *ad hoc* idea, but if we consider the order  $n = 6$  and  $n = 7$  on Fig.(14) the highest valued root in the region  $m^2 > 0$  from  $n = 7$  would need a root from  $n = 6$  to restore the right pattern, but apparently there is no such root. However, if we extend our picture with the compactified real line, we will see that in the region  $m^2 < -1$  the right root appears just where we would need it at order  $n = 6$  and thus the pattern goes on. This is true for all the other roots (Fig.(14)), thus the compactification of the real line is well justified in this way, hence providing us an  $M^*$  pattern on the compactified real line. On the interval  $[0, -1]$  one can now use the technique

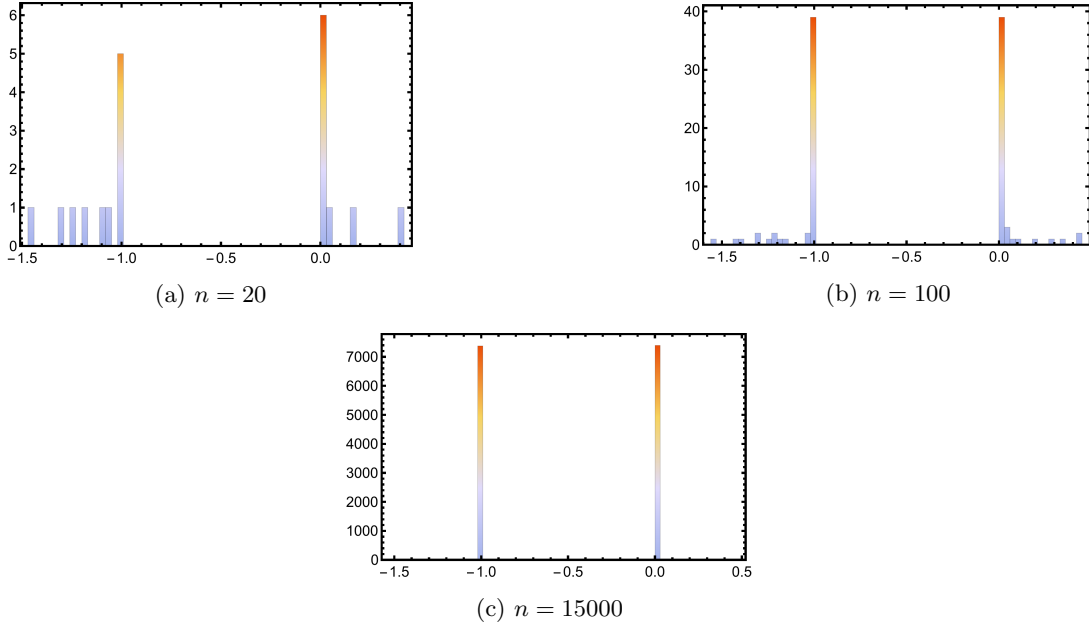


FIG. 15: Histograms of the distribution of the points generated in  $X_n$ . On the subfigure (a) the distribution of  $X_{20}$  on the subfigure (b) the distribution of  $X_{100}$  and on the subfigure (c) the distribution of  $X_{15000}$  are displayed. Note that the positions of the points are tending to  $-1$  and  $0$  but this time from the other side and at very high  $n$  the number of points between the two endpoints is negligible comparing to  $n$ , in other words: the probability of finding a point outside (and inside) when  $n \rightarrow \infty$  is zero.

we introduced in Section III. The result of such kind of random number procedure is shown on Fig.(15). We can see that the position of the roots again accumulating at  $-1$  and  $0$  but now they are approaching from the complement interval of  $(-1, 0)$ . In this way we can see how the triviality is emerging in the  $n \rightarrow \infty$  limit.

### B. Triviality for $O(N)$ theories in $D = 4$

In this section we are going to discuss the  $D = 4$  theories and a special attention will be given to the case  $N = 1$ , which has been in the centre of interest since triviality is suggested to the  $\phi^4$  theory. To have a clue on triviality beyond perturbation theory we still need to rely on lattice simulations which underpins the trivial behaviour of such theories [12]. Here we are going show a result which suggests that indeed the trivial scenario holds for such models, i.e. no UV fixed point different from the Gaussian is present in the  $O(N)$  models taking into account all the symmetry respecting terms in four dimensions (the  $\phi^4$  case is shown on Fig.(11)). We are going to present the result for  $N = 1$  but this holds for general  $N$ . The VBF polynomials for  $D = 4$  have the form:

$$\lambda_n \propto (-1)^{n+1} (m^2)^{1+\Theta(n-3)} (1+m^2)^n \sum_{i=0}^{n-2} g_i(N, D=4) (m^2)^{i-\Theta(n-3)}. \quad (27)$$

In particular for the first few  $\lambda_i$  for  $N = 1$ :

$$\begin{aligned} \lambda_2 &= -\frac{64\pi^2}{3} m^2 (m^2 + 1)^2, \\ \lambda_3 &= \frac{8192\pi^4}{5} (m^2)^2 (m^2 + 1)^3, \\ \lambda_4 &= -\frac{524288\pi^6}{35} (m^2)^2 (m^2 + 1)^4 (14m^2 - 1), \\ \lambda_5 &= \frac{67108864\pi^8}{315} (m^2)^2 (m^2 + 1)^5 (168(m^2)^2 - 41m^2 + 1), \\ &\dots \end{aligned} \quad (28)$$



By analysing the root structure of these equations one will find that all the roots are situated outside the interval of  $(-1, 0)$  likewise for the cases when  $D > 4$ , the only difference is that at the order  $n = 7$  the VBF curve  $\lambda_7$  develops a roots on the complex plane, too, with  $\text{Re } m^2 > 0$ . We have already met such situation at the theories which were defined in  $2 < D < 4$  dimensions. In that case we neglected these roots since we considered them as unphysical. In the present case we still stick to our convention, that is we neglect them as possible fixed point candidates, however we can identify an interesting behaviour for such non-real roots. Let us look at the root structure of the theory on Fig.(17), where we present the position of the real roots for all relevant intervals of  $m^2$ . What we can observe is that

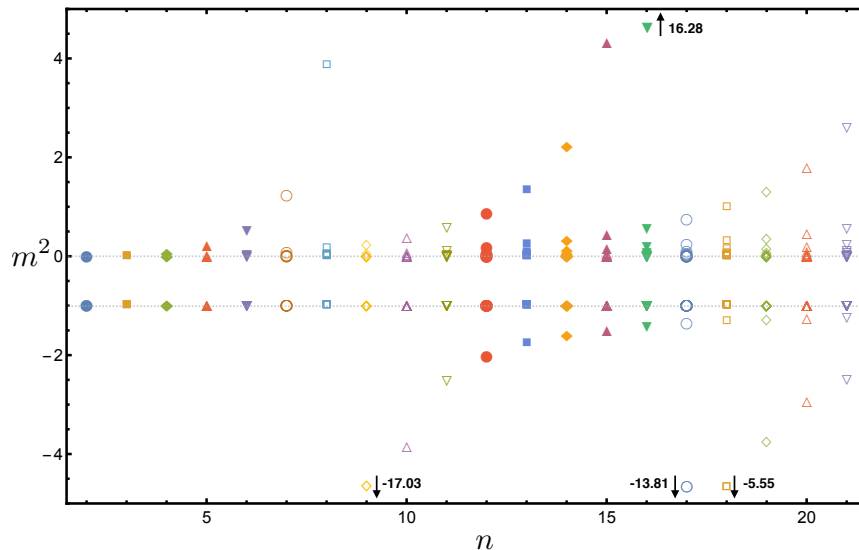


FIG. 16: The real roots of the four dimensional  $O(N)$  model are shown. No root in the interval  $(-1, 0)$  is found, contrary: all roots are outside this interval. One can see, just like in the case of the  $D > 4$ , that the roots are approaching  $-1$  and  $0$  from outside. However, more careful analysis is needed in this case. For details see the text.

the roots are approaching the points  $-1$  and  $0$ , just like in the case for  $D > 4$ . However, as we indicated above, complex roots are emerging: the first one and its conjugate from  $n = 7$ , two and their conjugates from  $n = 11$ , three and the conjugates from  $n = 15$  and from  $n = 18$  four complex roots plus conjugates. Among these roots, being complex, we cannot make an ordering, however we are able to do that for the real part of them. The real part of the roots are indicated on Fig.(17), complex roots with negative real parts does not occur, hence it is enough to consider the  $\text{Re } m^2 > 0$ . The figure shows that the for the real part of the roots, there is indeed a pattern, namely almost the same that we observed both for the cases  $D \leq 2$  and  $D > 4$ , the only differences are in the orders where the complex roots appear. Here we observe that above and below the real part of the newly appearing complex roots the pattern continues, only at those particular points we find the breaking of the pattern (these are indicated by red circle on Fig.(17)): no root from real part of the  $\lambda_{n+1}$  goes between the corresponding roots of  $\lambda_n$ . Now, if we consider the limiting distribution of such pattern of points, we will find this behaviour will not have an effect on it: after compactification of the real line, as we did it for the  $D > 4$ , the points are just accumulating at  $-1$  and  $0$ , hence we will find exactly the same result as in Eq.(20), but now only for the real part of  $m^2$ . We are not done yet, since we have only considered the real part so far. This result on the limiting position of the roots does not make any sense if we find a finite imaginary part of  $m^2$  in this limit. Let us consider therefore the roots on the complex plane. This is shown on Fig.(18). We can see the developing imaginary part at the order  $n = 7$  for the first time. Interestingly the absolute value of this imaginary part will have a maximum at some point and it is tending to zero just like the real part. We can also express the imaginary part as a power law of the real part close to the origin:  $\text{Im } m^2 = \pm a(\text{Re } m^2)^b$ , where the parameters  $a = 0.162 \pm 0.001$  and  $b = 0.589 \pm 0.001$ . Now, considering the "running" of the second and the third complex root ( $m_2^2, m_3^2$ ), which are appearing first at the order  $n = 11$  and  $n = 18$ , respectively, we will find that they behave in a very similar way to the first complex root ( $m_1^2$ ), moreover they collapse onto each other close to the origin (see Fig.(18)), thus approaching  $0$  with the same exponent. We can see that both the real and the imaginary parts of the roots are approaching zero as the order  $n$  grows, hence we can say that the roots, although they are not defined as physical ones when they have complex values, accumulating at  $-1$  and  $0$  in the  $n \rightarrow \infty$  limit. It is interesting that only in the limit the imaginary part is absent entirely and until we take this limit we will have a gap between  $m^2 = 0$  and the last non-complex valued root in the particular order  $n$ . With this procedure we were able

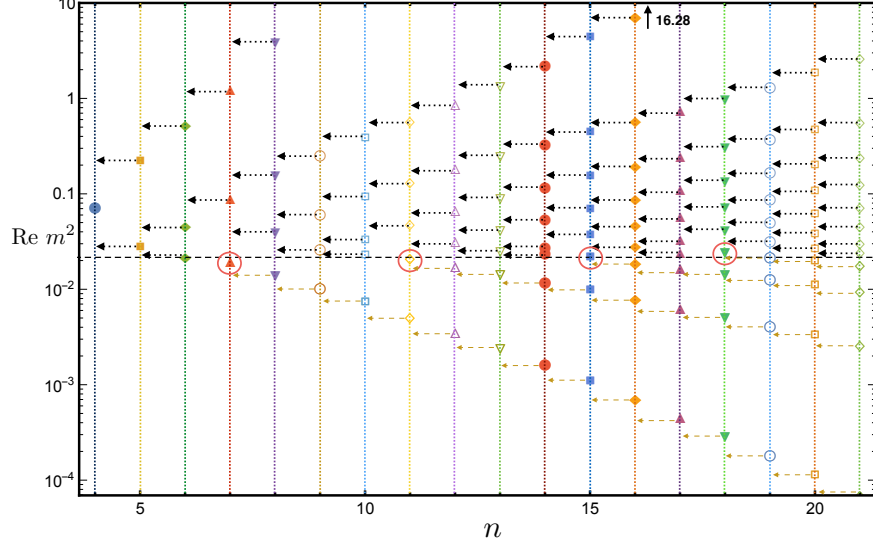


FIG. 17: The real part of the roots. The black dashed line indicates the average threshold between the purely real and complex root values. It is at about  $m^2 = 0.022$ . For every value of  $\text{Re } m^2$  under this line we have an imaginary part for the root. New complex roots are emerging at order  $n = 7$ ,  $n = 11$ ,  $n = 15$  and  $n = 18$ . At these orders we can see a "breaking of the pattern" which is being indicated by the arrows: pointed black arrows for the purely real and dashed gold for the complex roots. Apart from the newly emerging complex roots the pattern holds. For details see the text.

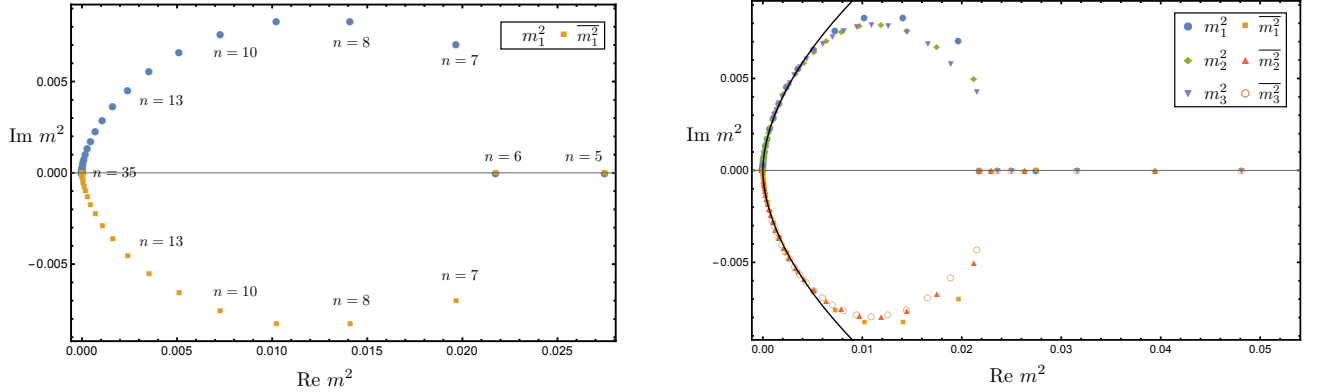


FIG. 18: The roots on the complex plane. On the upper panel one can see the emergence and disappearance of the first complex root ( $m_1^2$ ). It appears at  $n = 7$  and tends to zero as we go higher orders in  $n$ . On the lower panel the second and third complex roots are indicated ( $m_2^2$  and  $m_3^2$ ). They appear at order  $n = 11$  and  $n = 15$  respectively, and coincide with the curve defined by the complex root  $m_1^2$ . The fitted power law curves are defined in the text.

to show that only two fixed points are present (with the Gaussian as the only stable one) in the unexpanded  $O(N)$  theory just like for  $D > 4$ . This signals the triviality for the  $O(N)$  theories when the dimension is  $D \geq 4$ . Hence we were able to show a non-perturbative evidence of the triviality for theories defined in  $D \geq 4$ .

Regarding to the  $D = 3$  case in Section IV the roots on the complex plane does not behave in the way they do in the four dimensional case (Fig.(18)), hence we cannot obtain the distribution of the roots by using the random number generating algorithm for the compactified  $M^*$  pattern.

## VI. THE $N$ DEPENDENCE AND THE LARGE $N$

In this section we are going to show what is the effect of changing the number of fields, i.e.  $N$ , for particular dimensions. We can even calculate the limit when  $N \rightarrow \infty$ , which turns Eq.(7) into the following RG equation for the dimensionless effective potential:

$$\partial_t u = (D - 2)u' \rho - Du + \frac{A_d}{1 + u'}. \quad (29)$$

From this equation one can derive the VBF curves with the usual steps just the  $N$  dependence is absent from the formula Eq.(14). In this section we cannot show of course the full  $N$  dependence, these are only a few checks for particular values of  $N$ . One should derive the root structure for each  $N$  independently. However these few examples could give us some idea what is going on when  $N$  is being changed.

### A. $N$ dependence for $O(N)$ theories in $D \leq 2$

Let us consider three different two dimensional theories with finite  $N$  ( $N = 7$  and  $N = 15$ ) and the large  $N$  case, in order to have a clue on the  $N$  dependence of the VBF curves. The position of their roots are shown on Fig.(19). We can see in the two finite  $N$  cases that there seems to be a problem in the low orders of the expansion: the position of the roots will not satisfy the requirement of the  $M^*$  pattern, however, as the order grows the pattern restores. We

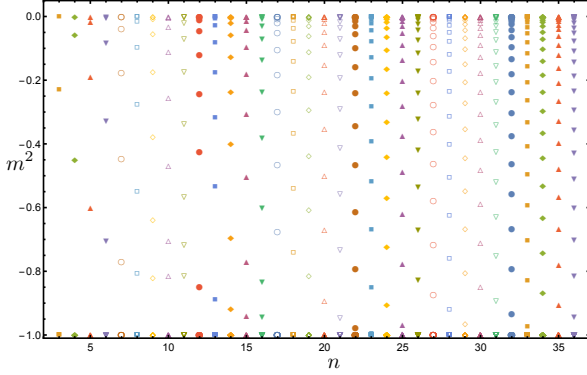
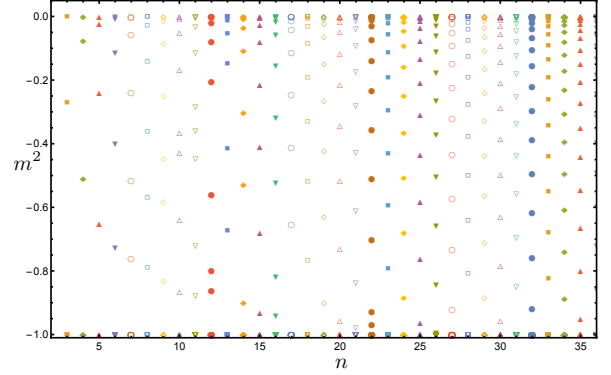
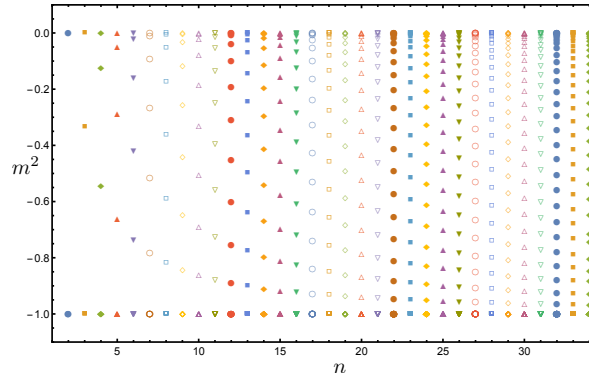
(a)  $N = 7$ (b)  $N = 15$ (c)  $N \rightarrow \infty$ 

FIG. 19: The  $N$  dependence of the root positions in  $D = 2$ . We can see that the right pattern restores at larger order of the expansion for various  $N$ . Sometimes one will find complex roots close to  $-1$  which can be considered as unphysical. In this way it does not actually matter if we consider the limit of the distribution of the roots or it gets complex providing an unphysical situation. When the  $n \rightarrow \infty$  limit is taken the only two roots that can be found is  $-1$  and  $0$ . In the large  $N$  no complex valued root has been found till the order  $n = 34$ .

need to mention that when a particular root gets very close to  $-1$  in the next order sometimes it becomes complex, but its real part still stays around  $-1$ , hence one cannot see this accumulation exactly, but rather we can say this root "melted" into  $-1$ . This might be related to the fact what we already explained for the  $D = 3$  case: the VBF polynomials get extremely flat close to  $-1$  because of the  $(1 + m^2)^n$  factor in Eq.(14), hence it could mean some problem for the root finding algorithm to provide the right value. One way or another, a complex root does not define a physically sensible theory thus we can still look at this pattern which will provide Eq.(20) as the probability density of the root positions when  $n \rightarrow \infty$ . However, no complex roots occur for the large  $N$  case where we know there must be only the symmetric phase that exist, as it was proven analytically in [22] in the framework of FRG. The fact that a root gets complex or accumulates at one of the stable fixed points  $-1, 0$  is irrelevant in the point of view of the physics: in both of the cases only  $-1$  and  $0$  survive when  $n \rightarrow \infty$ . For  $D = 1$  we can find similar results. These were of course only a few checks on the  $N$ -dependence and it should be considered case by case for every  $N$ , however from our experience we could assume that in the  $n \rightarrow \infty$  roots inside the interval  $(-1, 0)$  either get complex or they are arbitrarily close to  $-1$  or  $0$  for any  $N$ .

### B. $N$ dependence for $O(N)$ theories in $2 < D < 4$

In dimensions  $2 < D < 4$  for finite  $N$  we will get a very similar result to the one which we obtained in Section IV. For these values of the dimension one has the richest fixed point structure of all, hence it should be checked case by case, however here we will only concentrate on the integer valued dimension  $D = 3$ . For the large  $N$  in  $D = 3$  the position of the VBF roots show a significant difference comparing them to the finite  $N$  (compare Fig. (20) and Fig.(8)). Here we can identify the Wilson-Fisher just as we did it in Section IV but in this case we cannot see the additional "fake" fixed points at any truncation level. Also for the  $m^2 > 0$  roots we can see differences: they start to be organised in the pattern which leads us to the distribution found in Section III, Eq.(20). In this case it is also remarkable that no complex roots are found unlike for finite  $N$ .

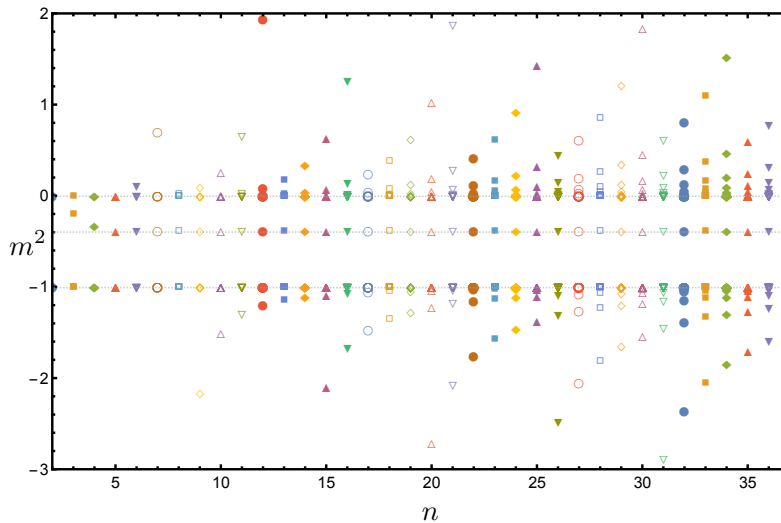


FIG. 20: The roots of the VBF in the  $D = 3$ ,  $N \rightarrow \infty$  are shown. Comparing it to Fig.(8) the most striking difference is that there are no "fake" roots between the root which is indicating the Wilson-Fisher ( $m^2 = -0.388$ ) and the one which is for the Gaussian, i.e.  $m^2 = 0$ . It is equally interesting that in this case we do not find any threshold which after the roots become complex in the  $m^2 > 0$  region.

### C. $N$ dependence for $O(N)$ theories in $D \geq 4$

One of the most important result for theories  $D \geq 4$  was the triviality (Section V). Our finding is that the modification of the number of the field components  $N$  does not give any qualitatively different result for any such theory, when

$N$  kept finite. However, we can discover differences between the results when  $N < \infty$  and  $N \rightarrow \infty$  for theories in  $D > 4$ .

1.  $N$  dependence for  $O(N)$  theories in  $D = 4$

In four dimensions we will see the "compactified"  $M^*$  pattern of the roots as on Fig.(17), the only question is whether the convergence on the complex plane towards the origin still holds. We present the results on Fig.(21), for  $N = 4$ ,  $N = 15$ ,  $N = 40$  and  $N \rightarrow \infty$ . We can observe that the convergence to the origin slows down as  $N$  grows,

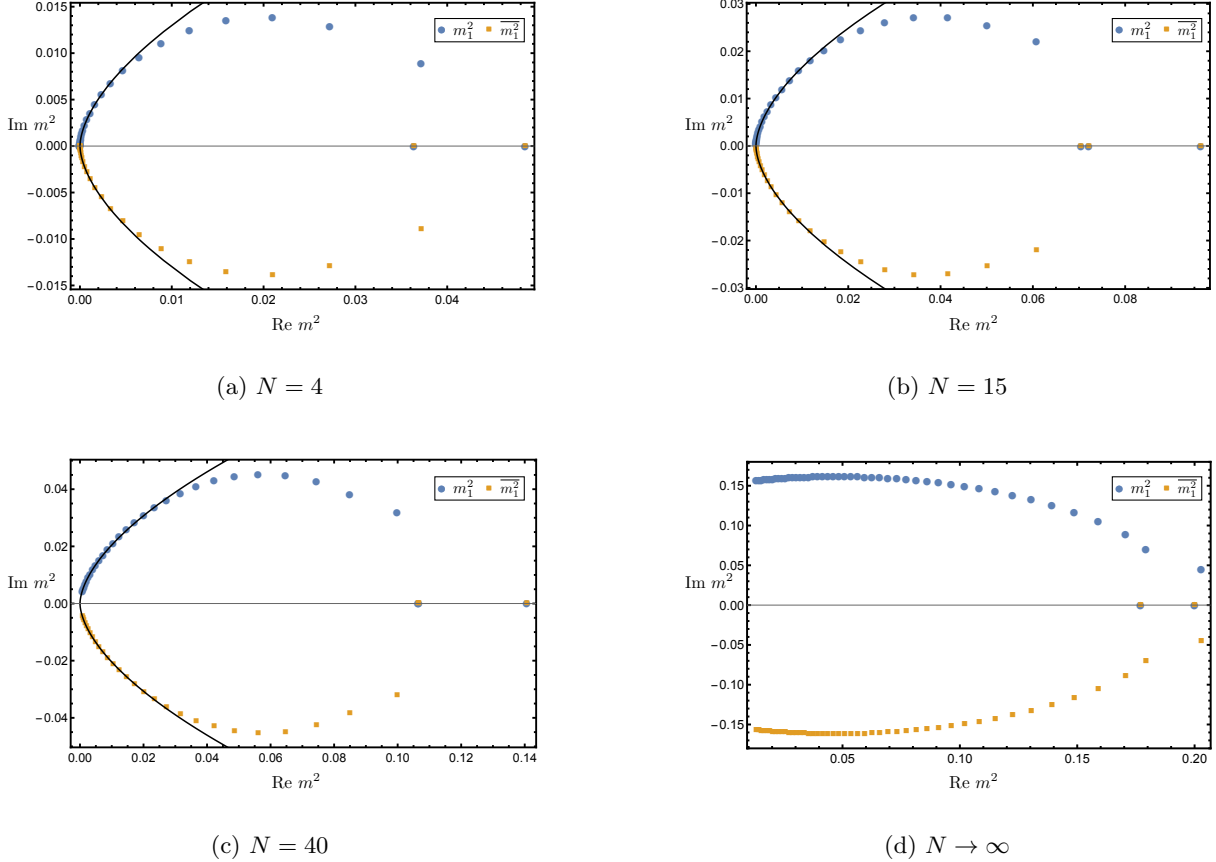
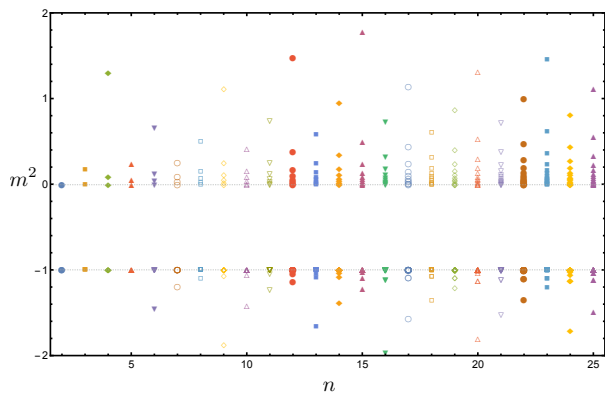


FIG. 21: The convergence to the origin on the complex plane is shown for (a)  $N = 4$ , (b)  $N = 15$  and (c)  $N = 40$ . On the figure (d) the  $N \rightarrow \infty$  presented, in this case the number of the data points is not enough to fit a curve on the points near the origin (the expansion order in this case  $n = 53$ , for the finite  $N$  cases  $n = 35$ ). However, the same behaviour is expected: the convergence to the origin slows down as  $N$  grows. For the finite  $N$  cases a power law fit could be found around the origin, which exponent seems to be universal. For details see the text.

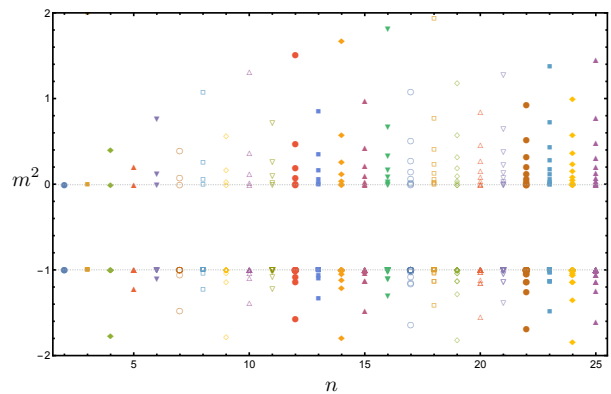
however for the  $N < \infty$  cases it is possible to fit a curve on them near the origin. The same form of the power law is found for each  $N$ , that is  $f(x) = ax^b$ , just like in the case of  $N = 1$  in Section V. The parameters are the following  $a = 0.193 \pm 0.001$ ,  $b = 0.587 \pm 0$  for  $N = 4$ ,  $a = 0.249 \pm 0.002$ ,  $b = 0.586 \pm 0.002$  for  $N = 15$  and  $a = 0.302 \pm 0.006$ ,  $b = 0.584 \pm 0.004$  for  $N = 40$ . It is interesting that close to the origin the exponent of the power law seems to take the value  $\approx 0.586 \pm 0.002$ , and thus one can speculate whether it is universal. Regarding the  $N \rightarrow \infty$  case we did not reach the region where we could do the fit, however, the absolute value of the imaginary part reached its maximum and started to decrease. We expect the same behaviour (maybe with different exponent) as for the finite  $N$  cases but to see that we would need to go to a higher expansion order than that has been used in this case ( $n = 53$ ).

2.  $N$  dependence for  $O(N)$  theories in  $D > 4$

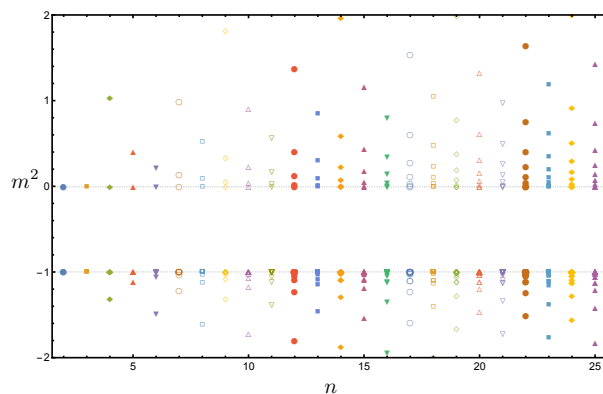
For theories in greater than four dimensions the fixed point structure does not change much comparing to the results of Section V, only quantitative differences can be observed. We will present a few plots about the roots positions on Fig.(22). Arbitrarily we have chosen the cases  $D = 5, N = 6$ ,  $D = 8, N = 10$  and  $D = 11, N = 12$ . The roots are positioned in a way that they accumulate more and more at the two stable roots  $-1$  and  $0$ , which is essential for triviality. There can be minor deviation from the pattern  $M^*$  which would lead us to the distribution of the roots in Eq.(20). However, at some point the pattern restores completely and one can obtain the triviality in a way we did it for  $D = 5, N = 1$ . More interesting case that we can find is in the large  $N$  limit. From Eq.(29) one can derive again the VBF curves for theories  $D > 4$ . In the present section we are going to study only the  $D = 5$  theory for the large  $N$ . On Fig.(23) one can see the root positions for this model. The first thing that we can notice, there is a stable line at  $m^2 = 0.139$  which would signal a new fixed point solution for such theory. There has been a recent work ([13]) on the topic whether such fixed point exist in theories  $4 < D < 6$  and the answer was that if there is such fixed point it will provide an unphysical fixed point potential. In an earlier work [14] related to holography a similar conclusion was drawn. In the papers [15] an IR fixed point was found for an  $O(N)$  symmetric theory with  $N + 1$  scalars in  $D = 6 - \epsilon$  for sufficiently large  $N$  including a cubic interaction. It was argued that this IR fixed point of the cubic  $O(N)$  theory with  $N + 1$  scalars is equivalent to a UV fixed point of the  $O(N)$  model in the large  $N$ , which would imply an unexpected asymptotically safe behaviour of such theories. Now, since we have found such a fixed point we need



(a)  $D = 5, N = 6$



(b)  $D = 8, N = 10$



(c)  $D = 11, N = 12$

FIG. 22: The VBF roots of the  $O(N)$  theories: (a) in  $D = 5$  and  $N = 6$ , (b)  $D = 8$  and  $N = 10$ , (c)  $D = 11$  and  $N = 12$ . On each plot the accumulation of the roots at  $m^2 = -1$  and  $m^2 = 0$ . For the roots  $m^2 < -1$  there can be small deviation from the  $M^*$  pattern (most likely due to the extreme flatness of the VBFs around  $-1$ ), but at some point the pattern is restored.

to check if it gives a stable fixed point potential. Substituting the value  $m^2 = 0.139$  into the VBF polynomials will provide the exact value for the corresponding coupling at that fixed point, hence defining the fixed point potential. The finding is the following: the highest order in the expansion is  $n = 46$ , and what we get is  $\lambda_n(m^2 = 0.139) \leq 0$  for  $2 \leq n \leq 46$ . This signals that the fixed point potential defined by this root is unbounded from below in agreement with the findings in [13]. On Fig.(23) one can also observe that there is a gap between the root corresponding for this newly found unstable fixed point which can be filled in by considering the real part of the roots. On the same figure considering the right panel we can see how the real part of such roots behave. We can fit a power law decaying curve again on the real part of the first such root. This curve goes through on the line  $m^2 = 0.139$  and in the asymptotic limit goes to zero. The imaginary part behaves pretty much in the same way as it behaved for the  $D = 4$  case (see Fig.(21)). Here we can use the same argument that we did for  $D = 4$ ,  $N = 1$ : one needs to consider the positions of the roots on the complex plane in order to catch the physics behind. According to our finding the real part of these roots exhibit the same  $M^*$  pattern, hence for  $n \rightarrow \infty$  we can expect them to accumulate at  $m^2 = 0$ , leaving us with three fixed points which are defined by the roots:  $m^2 = -1$  (since for  $m^2 < -1$  the root structure is the same as it was for the finite  $N$  case),  $m^2 = 0$  and  $m^2 = 0.139$ . Out of these three roots only the Gaussian ( $m^2 = 0$ ) will provide a stable fixed point potential, thus triviality was found again.

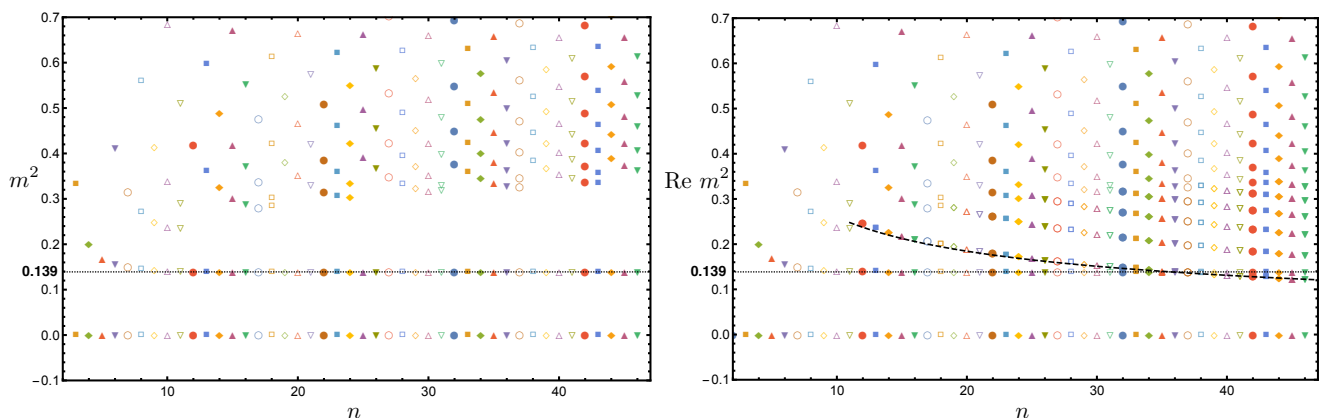


FIG. 23: On the left panel the root structure provided by the real roots are shown. A stable line of the roots can be observed at the value  $m^2 = 0.139$ . On the right panel the same root structure is shown but now the real part of the complex roots has been taken into account, too. The real part of the complex roots show the  $M^*$  statistics and also a power law function can be fit on the real part of the first such complex root  $f(x) = ax^b$ , with  $a = 0.807 \pm 0.005$  and  $b = -0.492 \pm 0.002$ . In the  $n \rightarrow \infty$  we expect to find triviality again. For details see the text.

## VII. THE FRACTAL DIMENSIONS

We will present a few example on the fractal dimensional cases in the intervals of the dimension that we have investigated. On Fig.(24) the results are shown for  $D = 1.3$ ,  $N = 1$ ,  $D = 2.6$ ,  $N = 1$ ,  $D = 3.1$ ,  $N = 1$  and  $D = 4.6$ ,  $N \rightarrow \infty$ . In the first three cases the usual fixed points are found, however it would be possible to find additional fixed points for  $2 < D < 4$  but that would require more detailed study of this interval of the dimension. For the two  $D$  values which are in this interval we found the Wilson-Fisher, too, and it can be observed that these are situated at different values of  $m^2$ : for  $D = 2.6$   $m_{WF}^2 = -0.34$  and for  $D = 3.1$  it oscillates around  $m_{WF}^2 = -0.16$ . The most remarkable case is the fourth when we set  $N \rightarrow \infty$  and chose  $D = 4.6 \in (4, 6)$ . Just as we saw it for the large  $N$  in  $D = 5$ , here we find again a fixed point candidate at the value  $m^2 = 0.108$ . However, again in agreement with [13], this fixed point found to be an unphysical one, i.e. the root  $m^2 = 0.108$  defines an unstable fixed point potential.

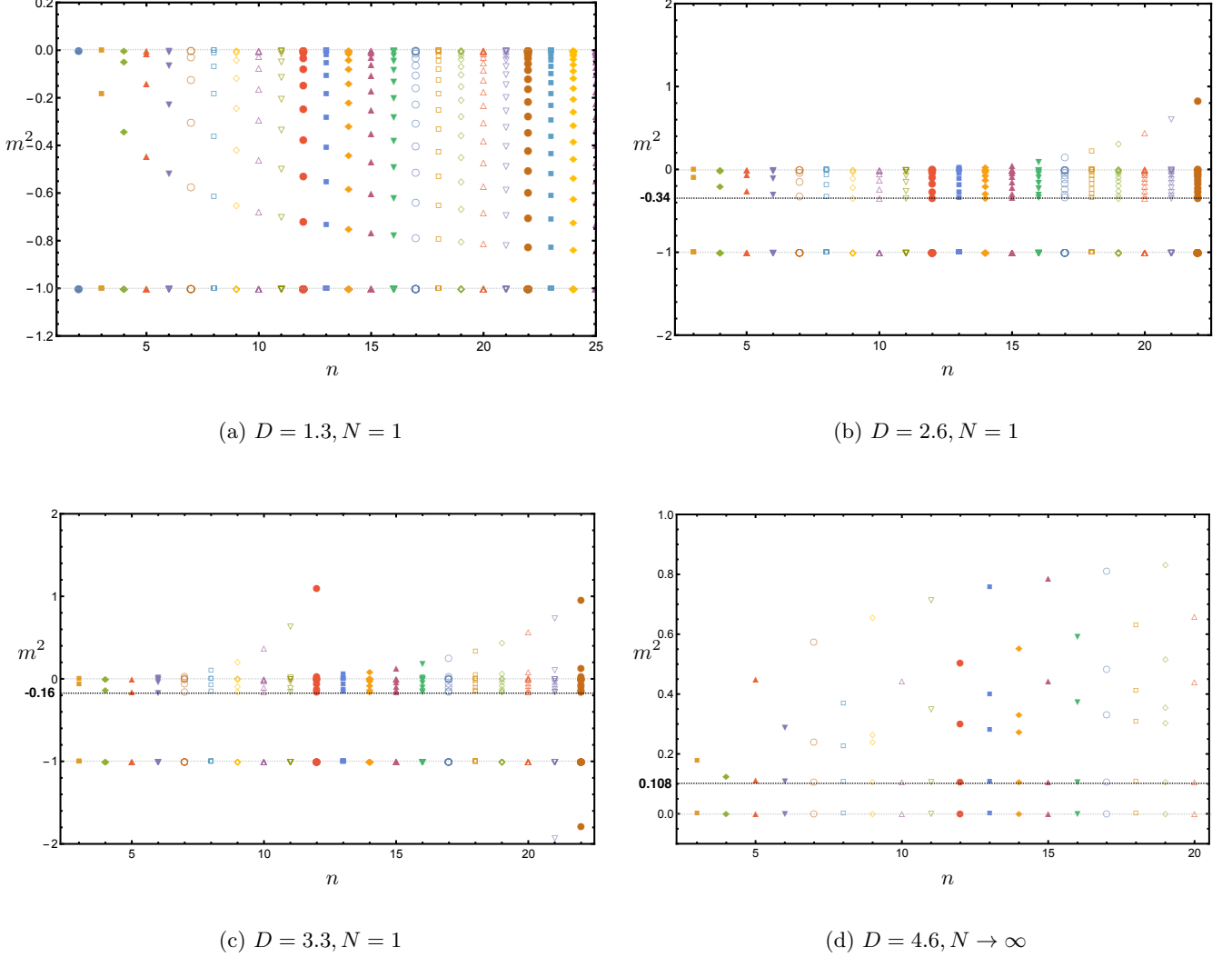


FIG. 24: The root structure is shown for the fractal dimensional cases. The usual fixed points are found, and the most remarkable is the figure (d), where we obtained a fixed point candidate for  $D = 4.6$  in the large  $N$ , but it turned out to define an unstable fixed point potential just like it is shown in [13].

## VIII. CONCLUSION

We investigated the fixed point structure of the  $O(N)$  model for various dimensions and field components. However in this paper we considered only the integer dimensional cases in details, but results for fractional dimensions are presented in the last section, too. For our analysis we used the Local Potential Approximation and the Taylor-expanded potential around vanishing field VEV. In this case from the fixed point equation one is able to express all the fixed point couplings through a polynomial in the mass of the theory, see Eq.(14). Each  $n$ th polynomial is obtained from the fixed point equation of the  $(n + 1)$ th coupling, that is the equation for  $\partial_t \lambda_{n+1}(\lambda_n, m^2) = 0$  can be solved for  $\lambda_n = \lambda_n(m^2)$ , hence the name VBF (Vanishing Beta Function) curve. A general property of these polynomials are that they have always a root at  $m^2 = -1$  and  $m^2 = 0$  corresponding to the convexity and the Gaussian fixed point, respectively. These polynomials can be obtained for arbitrarily  $N$  and dimension. To find a true fixed point at a given level of truncation we established the following rule: let  $m_0^2$  be a root of the polynomial  $\lambda_n(m^2)$ , then a physically well defined (i.e. bounded from below) fixed potential is given by the set of couplings  $\{\lambda_{n-1}(m_0^2), \lambda_{n-2}(m_0^2), \dots, \lambda_1(m_0^2) = m_0^2\}$ , provided  $\lambda_{n-1}(m_0^2) \geq 0$  (if it happens to be a root for the  $(n - 1)$ th polynomial, too, then the same rule holds for the  $(n - 2)$ th polynomial, and so on). Using this rule to find fixed points at a truncation level  $n$  gave us a nice opportunity



to make considerations about theories in different dimensions.

First we considered theories for  $D \leq 2$ . Particularly we analysed the case of  $D = 2$  in detail but the finding is that for all the theories that we considered up to dimension two qualitatively behave in the same way for  $N \geq 2$ . In such theories for continuous symmetries the Mermin-Wagner theorem must hold. We provided a statistical approach to show the validity of the theorem by considering the statistics of the root patterns. It was found that for such systems ( $D \leq 2$ ) all the roots are in the closed interval  $[-1, 0]$ . Since at every truncation level a new root appears it seems to be paradoxical to prove the Mermin-Wagner theorem: we would not expect any root inside the interval but practically there appears (countably) infinite many. A true fixed point in this interval signals an SSB phase, hence the theory seemed to be violated. Apparently it turned out it is only the case for finite  $n$  truncation, but as  $n \rightarrow \infty$  we can recover the MW theorem, by simulating the position of the roots and derive their distribution in the infinite limit, see Section III. For discrete symmetry  $N = 1$  the  $O(N)$  model is equivalent to the Ising model which has an SSB phase in  $D = 2$ . This result is also shown as a part of the section.

In Section IV we investigated the theory for  $D = 3$  with  $N = 2$ , but in  $2 < D < 4$  the finding is that the theories that has been considered has similar properties. We found the an additional fixed point to the Gaussian and the IR fixed point, namely the Wilson-Fisher fixed point. Although these fixed points have been found we could not clearly analyse the root structure for the  $m^2 > 0$  region. Here complex roots has been found preventing us to apply the statistical model that we used in the two dimensional case. It is also possible to find more additional fixed points in this region of the dimension but it would require more detailed study. The main result of this section is to show the appearance of the Wilson-Fisher fixed point.

For  $D \geq 4$  we found two qualitatively different results, however, essentially they lead us to the same physics, namely to triviality, that is only the Gaussian fixed point exist for such models. For theories  $D > 4$  we analysed the  $D = 5$  case where the fixed point structure shows similarity to the  $D = 2$  case but now the roots only appearing outside the interval  $(-1, 0)$ , however for the the root pattern the statistical simulation can be used again if we compactify the real line of  $m^2$ . In this way triviality could be shown. The situation for  $D = 4$  is different: here we need to consider the complex roots that are appearing during the calculations but it can be shown both the real and imaginary part converge to the origin on the complex plane, hence providing triviality.

In Section VI we showed some results considering different values of  $N$ . The most interesting result is connected to the recent results in [13], where it was argued that in the  $O(N)$  model for  $N \rightarrow \infty$  the nontrivial fixed points that can be found in dimensions  $4 < D < 6$  is defining an unstable fixed point potential. We obtained the same result from our analysis. In the last section we gave some results for fractional dimensions obtaining similar behaviour to the integer dimensional cases.

According to our findings we can draw the conclusion that although we used the Local Potential Approximation during our computations it seems to be enough to obtain the right qualitative physical results (Mermin-Wagner theorem, the presence of the Wilson-Fisher fixed point and triviality) when one takes the truncation of the Taylor expansion to infinity. On the other hand one has to be careful with such expansions, since as we saw, at finite level of the truncation it can generate "fake" fixed points from the point of view of physics.

## ACKNOWLEDGEMENT

I would like to thank István Nándori and Antal Jakovác for the fruitful discussions. I am also grateful to Zsolt Pajor-Gyulai, Matteo Giordano, Zoltán Szőr and Ákos Nagy for the very useful comments. This research was supported by the European Union and the State of Hungary, co-financed by the European Social Fund in the framework of TAMOP-4.2.4.A/ 2-11/1-2012-0001 'National Excellence Program' and by the Hungarian National Fund OTKA-K104292.

- 
- [1] R. Guida, J. Zinn-Justin, J. Phys. A **31**, 8103 (1998); J. Zinn-Justin, Phys. Rept. **344**, 159 (2001); B. Delamotte, D. Mouhanna, M. Tissier, Phys. Rev. B **69** 134413 (2004); J. M. Caillol, Condensed Matter Physics **16**, 43005 (2013); N. Dupuis, Phys. Rev. E **83** 031120 (2011); V. Branchina, E. Messina, D. Zappala, Int. J. Mod. Phys. A **28** (2013) 1350078.; D. Zappala, Phys.Rev. D **86** (2012) 125003; D. F. Litim, Dario Zappala, Phys. Rev. D **83**, 085009 (2011);
- [2] S.B. Liao, J. Polonyi, M. Strickland, Nucl. Phys. B **567**, 493 (2000); D. F. Litim, Nucl.Phys. B **631**, 128 (2002); D. F. Litim, JHEP **0507**, 005 (2005); C. Bervillier, B. Boisseau, H. Giacomini, Nucl. Phys. B **789**, 525 (2008); C. Bervillier, B. Boisseau, H. Giacomini, Nucl. Phys. B **801**, 296 (2008); S. Nagy, Phys. Rev. D **86**, 085020 (2012); J. M. Caillol, Nuclear Physics B **865**, 291 (2012);
- [3] L. Canet, B. Delamotte, D. Mouhanna and J. Vidal, Phys. Rev. D **67**, 065004 (2003); *ibid*, Phys.Rev. B **68** 064421 (2003); L. Canet, Phys.Rev. B **71** 012418 (2005);

- [4] J.-P. Blaizot, R. Mendez-Galain, and N. Wschebor, Physics Letters B **632**, 571 (2006); F. Benitez, J.-P. Blaizot, H. Chate, B. Delamotte, R. Mendez-Galain, N. Wschebor, Phys. Rev. E **80**, 030103 (2009); F. Benitez, J.-P. Blaizot, H. Chate, B. Delamotte, R. Mendez-Galain, N. Wschebor, Phys. Rev. E **85**, 026707 (2012);
- [5] A. Kapoyannis and N. Tetradis, Phys. Lett. A **276**, 225 (2000); D. Zappala, Phys.Lett. A **290**, 35 (2001); S. Nagy, K. Sailer, Annals Phys. **326** (2011) 1839.
- [6] C. Wetterich, Nucl. Phys. B **352**, 529 (1991); *ibid*, Phys. Lett. B **301**, 90 (1993); N. Tetradis, C. Wetterich, Nucl. Phys. B **422** [FS], 541 (1994).
- [7] A. Ringwald and C. Wetterich, Nucl. Phys. B **334**, 506 (1990); U. Ellwanger, Z. Phys. C **62** 503 (1994).
- [8] T.R. Morris, Int. J. Mod. Phys. A **9**, 2411 (1994); T.R. Morris, Phys. Lett. B **329**, 241 (1994).
- [9] D. F. Litim, J. Pawłowski, in *The Exact Renormalization Group*, ed. Krasnitz *et al.* (World Scientific, Singapore, 1999), 168; C. Bagnuls, C Bervillier, Phys. Rept. **348**, 91 (2001); J. Berges, N. Tetradis, C. Wetterich, Phys. Rept. **363**, 223 (2002); J. Polonyi, Central Eur. J. Phys. **1**, 1 (2004); J. Pawłowski, Annals. Phys. **322** 2831 (2007); H. Gies, Lect. Notes Phys. **852**, 287 (2012); B. Delamotte, Lect. Notes Phys. **852** (2012) 49. O. J. Rosten, Phys. Rept. **511**, 177 (2012).
- [10] D. F. Litim, Phys. Lett. B **486**, 92 (2000); *ibid*, Phys. Rev. D **64**, 105007 (2001); *ibid*, JHEP **0111**, 059 (2001).
- [11] I. Nándori, S. Nagy, K. Sailer, A. Trombettoni, Phys. Rev. D **80**, 025008 (2009)
- [12] Ulli Wolf, Phys. Rev. D **79**: 105002 (2009)
- [13] R. Percacci and G. P. Vacca, Phys.Rev. D **90** (2014) 10, 107702
- [14] Xavier Bekaert, Euihun Joung, Jihad Mourad, Proceedings of the XVII European Workshop on String Theory (Padova, 5-9 September 2011), arXiv:1202.0543 [hep-th]
- [15] Lin Fei, Simone Giombi (Princeton U.) , Igor R. Klebanov, Phys.Rev. **D90** (2014) 025018; Lin Fei, Simone Giombi, Igor R. Klebanov, Grigory Tarnopolsky, arXiv:1411.1099v3 [hep-th]
- [16] J. Alexandre and J. Polonyi, Ann. Phys. **288**, 37 (2001); J. Alexandre, J. Polonyi, K. Sailer, Phys. Lett. B **531**, 316 (2002).
- [17] E. Marchais, "Infrared properties of scalar field theories", Ph.D. Thesis , 2012, University of Sussex
- [18] N. D. Mermin and H. Wagner, Phys. Rev. Lett. **17**, 1133 (1966).
- [19] P. C. Hohenberg, Phys. Rev. **158**, 383 (1967).
- [20] S. Coleman, Comm. Math. Phys. **264**, 259 (1973).
- [21] L. Onsager, Phys. Rev. **65** (1944) 117-149.
- [22] N. Defenu, P. Mati, I. G. Marian, I. Nandori, A. Trombettoni, arXiv:1410.7024 [hep-th].
- [23] A. Codello, G. D'Odorico, Phys.Rev.Lett. **110** (2013) 141601; A. Codello, N. Defenu, G. D'Odorico arXiv:1410.3308.
- [24] I. Nándori, JHEP **1304**, 150 (2013).
- [25] I. G. Máriań, U. D. Jentschura, I. Nándori, J.Phys. G **41** (2014) 055001.
- [26] I. Nándori I. G. Máriań, V. Bacsó, Phys. Rev. D **89** (2014) 047701.
- [27] Alessandro Codello, Giulio D'Odorico, Carlo Pagani, JHEP **1407** (2014) 040